Technical Report

INSTITUTES FOR ENVIRONMENTAL RESEARCH IER 21-ITSA 21

Electromagnetic Pulse Propagation in the Normal Terrestrial Waveguide Environment

J. RALPH JOHLER

DECEMBER, 1966

Boulder, Colorado

THE INSTITUTES FOR ENVIRONMENTAL RESEARCH

The mission of the Institutes is to study the oceans, and inland waters, the lower and upper atmosphere, the space environment, and the earth, seeking the understanding needed to provide more useful services. These research Institutes are:

- The Institute for Earth Sciences
  conducts exploratory and applied research in geomagnetism, seismology, geodesy, and related earth sciences.

- The Institute for Oceanography
  works to increase knowledge and improve understanding of the ocean and its interaction with the total physical environment of the globe.

- The Institute for Atmospheric Sciences
  seeks the understanding of atmospheric processes and phenomena that is required to improve weather forecasts and related services and to modify and control the weather.

- The Institute for Telecommunication Sciences and Aeronomy
  supports the Nation's telecommunications by conducting research and providing services related to radio, infrared, and optical waves as they travel from a transmitter to a receiver. The Institute is also active in the study and prediction of periods of solar activity and ionospheric disturbance.

Environmental Science Services Administration

Boulder, Colo.

U. S. DEPARTMENT OF COMMERCE
John T. Connor, Secretary
ENVIRONMENTAL SCIENCE SERVICES ADMINISTRATION
Robert M. White, Administrator
INSTITUTES FOR ENVIRONMENTAL RESEARCH
George S. Benton, Director

ESSA TECHNICAL REPORT IER 21-ITSA 21

Electromagnetic Pulse Propagation in the Normal Terrestrial Waveguide Environment

J. RALPH JOHLER

INSTITUTE FOR TELECOMMUNICATION SCIENCES AND AERONOMY
BOULDER, COLORADO
December, 1966

Contents

Preface

This work was sponsored[1] by the Mitre Corporation, Bedford, Massachusetts. Other pertinent information may be found in the following documentation already published or soon to be published:

a. "Propagation of an Electromagnetic Pulse from a Nuclear Burst", J. R. Johler, IEEE Transactions on Antennas and Propagation, (to be published).

b. "Electromagnetic Pulse Propagation in the Disturbed Terrestrial Waveguide Environment", J. R. Johler, U. S. Dept. of Commerce, ESSA Technical Report, IER-22 ITSA-22, December 1966.

c. "Propagation of the Ground Wave Electromagnetic Signal, with Particular Reference to a Pulse of Nuclear Origin", J. R. Johler and J. C. Morgenstern, Proc. IEEE 53, No. 12 (December, 1965).

[1] Purchase order M1023.

Electromagnetic Pulse Propagation in the Normal Terrestrial Waveguide Environment

J. Ralph Johler

The theoretical problem of predicting the effect of the propagation medium on the form or shape of the low frequency electromagnetic pulse of nuclear origin has been discussed in a previous paper. This paper presents some greater detail on this remarkable propagation phenomenon. Particular emphasis is placed on the construction of transforms (amplitude and phase of the propagation medium as a function of frequency) which can be employed to propagate theoretically almost any pulse shape.

The distinctive features of the propagated pulse at great distance from the source can be identified with particular reflection regions of the ground and the ionosphere along the path between the source and the observer.

Key Words: EM-pulse, EM-pulse of nuclear original, LF, VLF, ELF transient propagation, pulse propagation, transient propagation, transient response of terrestrial waveguide.

1. Introduction

In previous papers (Johler and Morgenstern, 1965; Johler, 1967) the propagation of the electromagnetic pulse of nuclear origin was considered both as a ground wave and as a sum of ground and ionospheric waves in the terrestrial waveguide. Furthermore, the engineering significance of the study for nuclear test detection was considered quantitatively. Although a particular pulse[1] was propagated to great distance in the terrestrial waveguide, the transforms (amplitude and phase of the propagation medium as a function of frequency) calculated in the analysis procedure can be used to propagate most any pulse. Thus, in addition to presenting more detail on the propagation of the nuclear

[1] For details on the observed waveform employed in this paper to illustrate pulse propagation, see Johler and Morgenstern (1965).

pulse in the normal environment, this paper presents detail on the transforms at various distances from the source.

2. Terrestrial Waveguide Propagation Formulas

In previous papers (Johler, 1966a; 1966b; 1967) two basic formulas were considered: (1) the series of zonal harmonics and (2) the wavehop integral equations. The relative merits of these methods have also been discussed in some detail in these papers. The analysis employed in this paper was developed with the aid of the integral formulas:

$$E_{r,0} = \frac{iI_0 \ell}{k_1^2 a^4} \frac{\mu_0 c}{8\pi} \int_c \frac{F(\nu)-\frac{1}{2})}{\cos \nu\pi} \zeta^{(2)}_{\nu-\frac{1}{2}}(k_1 a)\, \zeta^{(1)}_{\nu-\frac{1}{2}}(k_1 a)(1+R_{\nu-\frac{1}{2}})\, d\nu, \qquad (2.1)$$

$$E_{r,j} = \frac{iI_0 \ell}{k_1^2 a^4} \frac{\mu_0 c}{8\pi} \int_c \frac{F(\nu-\frac{1}{2})}{\cos \nu\pi} \zeta^{(2)}_{\nu-\frac{1}{2}}(k_1 a)\, \zeta^{(1)}_{\nu-\frac{1}{2}}(k_1 a)(1+R_{\nu-\frac{1}{2}})^j C_j\, d\nu, \qquad (2.2)$$

where $I_0 \ell$ is the dipole source intensity, ampere-meters. The vertical electric source dipole field, $E_{r,0}$, is the ground wave. Also, the fields $E_{r,j}$, $j = 1, 2, 3 \ldots$ represent waves reflecting from the ionosphere j-times while traveling to great distance in the terrestrial waveguide. In formulas (2.1) and (2.2),

$$F(\nu-\tfrac{1}{2}) = \nu(\nu^2 - \tfrac{1}{4})\, P_{\nu-\frac{1}{2}}(-\cos\theta)$$

where the distance, d, between source and observer is $a\theta$,

$$\zeta^{(1,2)}_{\nu-\frac{1}{2}}(z) = \sqrt{\frac{\pi z}{2}}\, H^{(1,2)}_{\nu}(z),$$

where $H^{(1,2)}_{\nu}(z)$ is a Hankel function of order ν, argument z of the first or second kind, and $P_n(z)$ is a Legendre function, $k_1 = \frac{\omega}{c}\eta_1$, where $f = \frac{\omega}{2\pi}$ is the frequency, a is the radius of the terrestrial sphere, $\mu_0 = 4\pi(10^{-7})$ henry/meter, η_1 = index of refraction (air $\sim$ 1.0001 to 1.0003) and c is the speed of light. The spherical reflection coefficient of the ground $R_{\nu-\frac{1}{2}}$ is given for the vertical electric polarization (TM-mode propagation in the terrestrial waveguide) as:

$$R_{e,n} = \frac{\frac{\zeta_{1a}^{(1)\prime}}{\zeta_{1a}^{(1)}} - \frac{k_1}{k_2}\frac{\zeta_{2a}^{(1)\prime}}{\zeta_{2a}^{(1)}}}{-\frac{\zeta_{1a}^{(2)\prime}}{\zeta_{1a}^{(2)}} + \frac{k_1}{k_2}\frac{\zeta_{2a}^{(1)\prime}}{\zeta_{2a}^{(1)}}}, \qquad (2.3)$$

where $n = \nu - \frac{1}{2}$ and the abbreviations $\zeta_{1a}^{(1,2)} = \zeta_n^{(1,2)}(k_1 a)$ and $\zeta_{2a}^{(1,2)} = \zeta_n^{(1,2)}(k_2 a)$ have been introduced. Here $\zeta_n^{(1,2)\prime}(z) = \frac{d}{dz}\zeta_n^{(1,2)}(z)$ and $k_2 = \sqrt{\epsilon_2 - i\frac{\sigma \mu_0 c^2}{\omega}}$, where ϵ_2 and σ are the dielectric constant and conductivity of the ground, respectively.

The factor, C_j, can be calculated from the ionosphere and ground reflection coefficient matrices, R_n and T_n,

$$R_n = \begin{bmatrix} R_e & 0 \\ 0 & R_e \end{bmatrix}, \qquad (2.4)$$

$$T_n = \begin{bmatrix} T_{ee} & T_{ea} \\ T_{ae} & T_{aa} \end{bmatrix}, \qquad (2.5)$$

$$\rho_n = p \begin{bmatrix} 1 & 0 \\ 0 & -R_e \end{bmatrix}, \qquad (2.6)$$

$$p = \frac{\zeta_{1a}^{(1)}}{\zeta_{1a}^{(2)}} \cdot \frac{\zeta_{1g}^{(2)}}{\zeta_{1g}^{(1)}}, \qquad (2.7)$$

where $g = a + h$ and h is the reflection height of the terrestrial waveguide. Then,

$$(\rho_n T_n)(R_n T_n)^{j-1} = p^j \begin{bmatrix} C_j & x_j \\ y_j & z_j \end{bmatrix}. \qquad (2.8)$$

The reflection coefficients, T_{ee}, T_{ea}, T_{ae}, and T_{aa} are calculated by the Johler and Harper (1962) method with complex angle of incidence on the ionosphere (Johler, 1966a),

$$\cos \varphi_i = i \frac{\zeta_{1s}^{(2)'}}{\zeta_{1s}^{(2)}} . \qquad (2.9)$$

The reflection coefficients, T_{ee}, T_{e2}, T_{2e}, T_{22}, also depend on the profile of the ionosphere (electron density, ion density, and collision frequency as a function of altitude) the magnetic azimuth, φ_a, the magnetic dip, I, and the magnetic intensity, $\mathcal{H}$. For details, see Johler and Harper (1962), Johler (1963).

It is, of course, noted that $n = \nu - \frac{1}{2}$ when equations (2. 3) to (2. 9) are employed in the integrals (2. 1) and (2. 2). The details on evaluating these integrals (2. 1) and (2. 2) have been thoroughly discussed by Berry (1964), Berry and Chrisman (1965), and computer programs to accomplish this evaluation are available.

An alternate approach to this problem has been given by Johler (1964, 1966a) in the form of the zonal harmonics series,

$$E_{r,0} = \frac{\mu_0 c}{8\pi} \frac{I_0 l}{k_1^2 a^2} \sum_{s=0}^{\infty} F(n) \zeta_{1s}^{(2)} \zeta_{1s}^{(1)} (1 + R_e), \qquad (2.10)$$

$$E_{r,j} = \frac{\mu_0 c}{8\pi} \frac{I_0 l}{k_1^2 a^2} \sum_{s=0}^{\infty} F(n) \zeta_{1s}^{(2)} \zeta_{1s}^{(1)} (1 + R_e)^2 p^j C_j, \qquad (2.11)$$

where $F(n) = n(n+1)(2n+1) P_n(\cos \theta)$. Whereas, it was anticipated that (2. 10) and (2. 11) would replace the former (2. 1) and (2. 2) as a consequence of greater flexibility and programming simplicity (a discussion of these matters have been given by Johler, 1966a), the former formulas (2. 1) and (2. 2) were employed, since the computer programs for the latter (2. 10) and (2. 11) were not complete at the onset of this task. However, a check was made by comparing the calculations based on (2. 1) and (2. 2) with calculations based on (2. 10) and (2. 11) and excellent agreement was found.

To completely define the pr mises of the calculations to be presented, the reader will be burdened with one additional mathematical co cept--the Fourier transform integral. Equations (2. 1), (2. 2), (2. 10), and (2. 11) satisfy Maxwell's equations in the terrestrial waveguid at any frequency, ω, as vertical electric components of the

field $\vec{E}(\omega, d)$, $\vec{H}(\omega, d)$. Quite generally (i.e., for linear amplitude restrictions) the Fourier transform-integral theorem can be employed to obtain solutions of Maxwell's equations, $\vec{E}(t', d)$, $\vec{H}(t', d)$ in the time, t, domain,

$$E(t', d) = \frac{1}{2\pi} \int_{-\infty}^{\infty} \exp(i\omega t') E(\omega, d) f_r(\omega) \int_{0}^{\infty} \exp(-i\omega t) F_s(t)\, dt d\omega, \tag{2.12}$$

where $f_r(\omega)$ is the transfer function of the receiver or measuring device, $F_s(t)$ is the transient dipole source current moment, and the local time, t', is defined,

$$t' = t - \eta_1 d/c. \tag{2.13}$$

In the equation (2.12), it is assumed that

$$E(\omega, d) = \sum_j E_j(\omega, d) \tag{2.14}$$

and the integration can be performed term-by-term before summation,

$$E(t', d) = \sum_j E_j(t', d). \tag{2.15}$$

These methods of transformation to the time domain have been described in detail by Johler (1962). The integral (2.12) is complex. Ordinarily, the waveform, Re $E(t', d)$ is or primary interest (Re designates the "real part of"). The modulus, $|E(t', d)|$, describes an envelope of the pulse. Also, a perfect receiver will be assumed in (2.12), $f_r(\omega) = 1$.

Consider an experimental situation in which a waveform is observed and recorded at a short distance (ground wave distance), d_1, from the source. After digitizing the waveform, Re $E(t', d_1)$ a transformation on the computer can be made,

$$F_0(\omega, d) = \int_{0}^{\infty} \exp(-i\omega t)\ \mathrm{Re}\ E(t', d_1)\, dt. \tag{2.16}$$

To propagate the waveform theoretically on the computer to a great distance, d_2, the transforms $E_0(\omega, d_1)$ and $E(\omega, d_2) = \sum_j E_j(\omega, d_2)$ are required. The predicted waveform at d_2 is then,

$$\mathrm{Re}\, E(t', d_2) = \sum_{j=0}^{\infty} \frac{1}{2\pi} \int_0^{\infty} \exp(i\omega t') \frac{F_0(\omega, d_1)}{E_0(\omega, d_1)} E_j(\omega, d_2)\, d\omega, \quad (2.17)$$

where the integration can be performed term-by-term and summed, after an interchange of the order of summation and integration.

3. Discussions Concerning the Transforms

The geometric-optical theory is a useful adjunct for any discussion of the rigorous theory employed in the calculations. The rays corresponding to the rays of the geometric-optical theory (Johler, 1962) are depicted in figure 1. The rigorous theory has been expressed in (2.1), (2.2), (2.10), and (2.11) as the series,

$$E_r(\omega, d) = \sum_{j=0}^{\infty} E_{r,j}(\omega, d). \quad (3.1)$$

Geometric optical rays (the principal rays) corresponding to each term of this rigorous series (Johler, 1964) can be identified with regions of reflection near the points [1, 1], [2, 1], [2, 2], [3, 1], [3, 2] $\cdots$ in figure 1. The angle of incidence on the ionosphere is at a particular value, n, the real part of φ_1 in (2.9), and is a geometrical angle which the ray makes with the vertical direction. The precision calculations used in the rigorous theory employ the complex angle of incidence, both at the ionosphere and the ground.

At each point [1, 1], [2, 1], [2, 2], [3, 1], [3, 2] $\cdots$, a profile is introduced to determine the reflection process. A typical profile for daytime-noon conditions of the ionosphere is illustrated in figure 2. Here both the ion and electron density are shown. However, at frequencies greater than approximately 1 kc/s, for the particular case of the normal daytime ionosphere only the electrons need be considered. In a disturbed or nuclear environment this is no longer true. Thus, ion densities between 10^4 and 10^5 below 60 km can be induced by natural x-rays or x-rays and β-rays from a high altitude nuclear detonation. Johler and Berry (1965) have introduced this analysis into the general propagation theory, and details can be obtained from their paper.

The reflection coefficient (amplitude and phase) as a function of the angle of incidence, $\varphi_i = \text{Re Arc cos}\left[i \frac{\zeta_n^{(2)'}(k_1 g)}{\zeta_n^{(2)}(k_1 g)} \right]$ is given in figures 3 and 4. Thus, the real part of the angle of incidence can be interpreted as a geometrical angle of incidence on the ionosphere. Note that $T_{\theta\theta}$ and $T_{\phi\phi}$ approach -1 at grazing incidence, $\varphi_i = 90°$, and $T_{\theta\phi}$ and $T_{\phi\theta}$ vanish. The pseudo-Brewster angle of $T_{\theta\theta}$ (vertical electric polarization of the incident and reflected waves) is evident at approximately 50° as an inflection in the curve $|T_{\theta\theta}|$ as a function of φ_i.

The calculation of the reflection coefficients also employed a profile of collision frequency used by Johler and Berry (1965),

$$\nu(h) = 1.6(10^{11}) \frac{P(h)}{P_0} \quad , \tag{3.2}$$

where P(h) is the pressure at height, h, above the surface of the earth as given by the standard model atmosphere (U. S. Standard Atmosphere, 1962) and P_0 is the pressure at sea level.

The propagation in the ionosphere assumed the following magnetic parameters:

$|\mathcal{H}| = 40$ A/m

$\varphi_H = 270°$ (magnetic azimuth, the propagation into the West)

$I = 60°$ (the magnetic dip).

Obviously, other magnetic parameters can be selected, but this rapidly generates large volumes of data, whereas in this paper we wish to demonstrate principles of pulse propagation.

As a consequence of the calculation of reflection coefficients by the Johler-Harper (1962) method, the transmission into the ionosphere can also be described as a by-product of this analysis. This also gives an estimate of the effective height, h, of the upper boundary of the ionosphere emplaced at g = a + h relative to the center of the terrestrial sphere. This effective height of the upper boundary of the waveguide can be estimated from the transmission coefficient curves depicted, for example, in figures 5 and 6. Let $E_{y,i}$ be the normal

component of the incident electric field in the plane of incidence (vertical polarization) and let $E_{x,i}$ be the component perpendicular to the plane of incidence (horizontal polarization). Let $E_{y,u}$ and $E_{x,u}$ be the corresponding upgoing waves inside the ionosphere and $E_{y,d}$ and $E_{x,d}$ be the downgoing waves. Then, using the transformed coordinates of Johler and Harper (1962), $\hat{x}$ and $\hat{y}$, the ratios

$\frac{E_{\hat{x},u}}{E_{\hat{x},i}}$ and $\frac{E_{\hat{y},u}}{E_{\hat{y},i}}$ describe the propagation of waves into the ionosphere. In such a formulation, the transmission coefficient, U_e, for vertically polarized waves is given by the quantity

$$U_e = \frac{E_{y,u}}{E_{\hat{y},i}} \quad , \tag{3.3}$$

or (Johler and Berry, 1965),

$$U_e \sim \frac{E_{\hat{y},u}}{E_{\hat{y},i}} \cos\varphi_i \cos\varphi_a . \tag{3.4}$$

Thus, for the case $\varphi_a = 270°$, $U_e \sim 0$. In fact, U_e is very small at the bottom of the ionosphere for the upgoing wave in figures 5 and 6. The transmission coefficient, U_e, is finite as a consequence of the coupling between propagation components U_e and U_a within the ionosphere. In short (3.4) is an equality only in an isotropic plasma. In an anisotropic plasma there are small additional terms caused by the anisotropy.

The transmission coefficient, U_a, for the horizontally polarized incident wave can be written,

$$U_a = \frac{E_{y,u}}{E_{\hat{x},i}} \quad , \tag{3.5}$$

or, again,

$$U_a \sim \frac{E_{\hat{x},u}}{E_{\hat{x},i}} \sin\varphi_a . \tag{3.6}$$

Thus, the transmission of the vertical electric polarization of the wave into the ionosphere can be conveniently studied when $\varphi_a = 270°$, while 90° is the most convenient for the horizontal electric polarization. Figures 5 and 6 for 10 kc/s and 100 kc/s, respectively, show the amplitude $|U_e|$ $|U_a|$ for both upgoing and downgoing waves as a function of distance, z, into the ionosphere (z is the distance from the assumed bottom of the profile, h = 40 km in figure 2. This point

should be chosen such that the ionization is negligible at the assumed frequency. The typical angle of incidence, φ_i is 82° (grazing incidence). Figures 5 and 6 show that $|U_{a,u}| \sim 1$ just inside the ionosphere, $z \sim 0$. Here virtually no energy has as yet reflected; the situation continues with only slight decrease in $|U_{a,u}|$ until the wave penetrates approximately 25 km into the ionosphere in both figures 5 and 6 (10 kc/s and 100 kc/s, respectively). There is then a sharp decrease in the next few kilometers that appears to be more precise at 100 kc/s. This sharp decrease in the field indicates a decrease in the upgoing energy. Hence, as far as the reflection coefficient is concerned, the greatest contribution occurs before the upgoing wave has diminished to negligible amplitude. At this point the transmission coefficient, $|U_{e,a}|$, has decreased only slightly from unity. A few kilometers beyond that point, $|U_{e,a}|$ diminished rapidly. It is apparent, in both figures 5 and 6, that the effective height of reflection lies between approximately $z \sim 20$ and $z \sim 30$ km and depends upon the precise ratio $|U|$ used to define such a point. The uncertainty of resolution of the point follows, of course, since some energy, however small, is reflected at all heights, z. The uncertainty is also somewhat greater at 10 kc/s than at 100 kc/s, since the sharpness of the steep part of the curve is less at the lower frequency. It can be concluded, however, that the approximate value for the waveguide height, $h \sim 65$ km. This value was employed in the analysis, since only a weak frequency dependence of the reflection heights thus defined exists. A decrease in the attenuation of the upgoing wave is reached at higher altitude (fig. 5, for example). Fortunately, the reflection coefficient is determined to the required accuracy before this point is reached. Otherwise, it is at least conceptually possible that more than a single reflection height could exist.

The propagation medium transform constructed from the above described model of the ionosphere is illustrated at a distance, d = 1609 km (1000 statute miles) from the source in figure 7 (amplitude) and 8 (phase). The amplitude (volts/meter) is normalized to unity source dipole current moment, $I_0 \ell = 1$ A/m. The ground wave, j = 0, and various ionospheric waves of importance, j = 1, 2, 3 ··· are shown together with the total field, Σ. Since the ions can be neglected in the normal ionosphere, an electron gas was used to calculate the reflection coefficients. As a check, however, several reflection coefficients were calculated employing both the ions and electrons illustrated in figure 2, together with the neutrals and corresponding negative ions obtained from the conservation of charge equation. Also, the corresponding 12 collision frequencies as described by Johler and Berry (1965) were introduced. The electron gas model was found to be sufficiently accurate for the normal daytime model in figure 2.

Figures 7 through 18 give the complex transforms of the propagation medium in the presence of the normal daytime-noon model ionosphere to great distance, 1609 km to 8046 km. Thus, in addition to providing transforms for the propagation of pulses, a survey of the propagation at frequencies < 300 kc/s is clearly shown. Although the pulses are summed $\sum_j E_j(t', d)$ in the time domain, the $\sum_j E_j(\omega, d)$ in the frequency domain provides information over the entire low frequency spectrum for CW type (continuous wave) propagation.

The form of the $\left|\sum_j E_j(\omega, d)\right|$ curve as a function of frequency is of particular interest, see figure 17, for example, representing propagation to a distance, d = 8046 km. If the propagation path were entirely in daytime noon conditions one could expect such a curve to represent the propagation medium. The crest of the spectrum is approximately 18 kc/s. Thereafter, on the high frequency side the attenuation of the wave is quite severe. On the low frequency side of the crest of the spectrum, waveguide cutoff causes some attenuation. However, near 3 to 5 kc/s a minimum is reached and the propagation recovers. This region 3 to 5 kc/s resembles a pseudo-Brewster angle phenomenon analogous to reflection from a dielectric or the behaviour of the reflection coefficient $T_{e\ell}$ previously discussed. This is caused, however, by the reflection coefficient of the ground $R_{e,n}$, (2.3) where the complex angle of incidence,

$$\cos \tau = i \frac{\zeta_n^{(2)}(k_1 a)}{\zeta_n^{(1)}(k_1 a)} ,$$

is a function of frequency. Details on this phenomenon have been given in a previous paper (Johler and Berry, 1964). The rather excellent propagation in the vicinity of 16 kc/s is herein substantiated theoretically.

The detail on the propagation at short distances (< 1609 km) was presented in two previous papers by Johler (1967) and Johler and Morgenstern (1965) and hence will not be treated here. Also, the former paper presented waveforms at great distance. In this paper we shall supplement those calculations with greater detail on the distances greater than 1609 km.

4. Propagation of the Pulse to Great Distances

The theoretical reconstruction of the pulse from a nuclear burst is illustrated at intermediate and great distances in figures 19 through 24. The waveform Re $E(t', d_2)$ is depicted for each term, $j = 0, 1, 2, 3 \cdots$ of the series (2.17) together with the sum Re $\sum_j E_j(t', d_2)$. Thus, for example, in figure 22, $d = d_2 = 4828$ km, the curve of the composite pulse is constructed by superposing the multiple ionospheric waves, $j = 0, 1, 2, 3, 4, 5$. The ground wave, Re $E_0(t', d)$ produces almost negligible ripple on this scale as shown by the long dash, two short dash, and long dash . . . curve. A small undulation represents the Re $E_0(t', d)$ + Re $E_1(t', d)$ as represented by the short dashed curve. The long dashed curve representing the sum Re $E_0(t', d)$ + Re $E_1(t', d)$ + Re $E_2(t', d)$ essentially establishes the second cycle of the pulse. The long dash, dotted curve essentially establishes the third cycle of the pulse as the sum Re $E_0(t', d)$ + Re $E_1(t', d)$ + Re $E_2(t', d)$ + Re $E_3(t', d)$. The dotted curve represents the sum Re $E_0(t', d)$ + Re $E_1(t', d)$ + Re $E_2(t', d)$ + Re $E_3(t', d)$ + Re $E_4(t', d)$. Finally, the $\sum_5 E_j(t', d)$ represents the first 300 μs of the pulse. For later times, higher ionospheric wave pulses may be required. However, these higher order pulses become highly attenuated in the propagation transforms considered in this paper. It is evident that the first cycle of the pulse between 0 and approximately 70 μs is essentially determined, figure 1, by a reflection from the ionosphere in approximately the region about the midpoint, [1, 1], of the propagation path. Between 70 and 110 μs, a reflection from the regions about $j = 2$ reflection points, [2, 1], [2, 2], determined essentially this portion of the pulse. Similarly, the other parts of the pulse can be associated with ionosphere regions along the propagation path.

Similar comments could be made at the various distances between 1609 and 8046 km. At the shorter distances only two or three terms j are required. Also, at distances greater than 4828 km, the ground wave is extremely small compared with the ionospheric waves.

The complete waveform, Re $\sum_j E_j(t', d)$, is depicted in figure 25 as a function of local time, t', at various distances between 1609 and 8046 km. The change in form or shape of the pulse as a consequence of the filtering action of the propagation medium is evident. Of particular interest is the sinusoidal nature of the propagated pulse which has been reconstructed by summing the geometric series. Thus, as the distance from the source becomes great the source becomes

obscured by the characteristic frequency of the propagation medium illustrated in figure 17, for example. Thus, at the greater distances the higher frequencies are even more severely attenuated.

5. Conclusions

The development of complex transforms for the terrestrial waveguide propagation medium is an extremely useful enterprise, since the complex transforms so constructed can be kept in permanent form and employed to propagate most any pulse with energy composition in the low frequency (< 1000 kc/s) domain.

At very great distances from the sources, the pulse is characterized in a large measure (but not completely) by the propagation medium frequency characteristic. In fact the pulse tends to become sinusoidal in nature as the higher frequencies are attenuated more severely at the greater distances.

A transient waveform reconstructed theoretically at great distance from the source can be analyzed with the aid of the Fourier transform-integral theorem applied to each term of the geometric series expansion of the terrestrial waveguide propagation formula. Different times on the pulse can be identified with particular reflection regions of the ground and ionosphere along the propagation path. At great distance from the source the pulse is primarily determined by the higher order terms of the geometric series, i.e., the pulse is propagated around the terrestrial sphere by successive reflections to and fro between the ionosphere and the ground.

The analysis presented in this paper suggests its use as a powerful tool for the understanding of D-region phenomena. Thus, physical changes along the propagation path can be identified as amplitude changes at different local time, t', on the pulse.

The author is indebted to Richard S. Greeley, Ted Jarvis, Laurence Jacobs, Nicholas Del Vecchio, John Morgenstern, and other members of the professional staff of the Mitre Corporation for many stimulating discussions which influenced the course of this work. The author acknowledges the able assistance of Carlene Lilley with the many details of the computer computation.

6. References

Berry, L. A. (1964), Waves hop theory of long distance propagation of LF radio waves, Radio Sci. J. Res. NBS 68D, No. 12, 1275-1282.

Berry, L. A., and M. E. Chrisman (1965), The Path integrals of LF/VLF wave hop theory, Radio Sci. J. Res. NBS 64D, 1469-1480.

Johler, J. R. (1962), Propagation of the low-frequency radio signal, Proc. IRE 50, No. 4, 404-427.

Johler, J. R. (1963), Radio wave reflections at a continuously stratified plasma with collisions proportional to energy and arbitrary magnetic induction, International Conference on the Ionosphere, London, July 1962 (The Institute of Physics and Physical Society, London), 436-445.

Johler, J. R. (1964), Concerning limitations and further corrections to geometric-optical theory for LF, VLF propagation between the ionosphere and the ground, Radio Sci. J. Res. NBS 66D, No. 1, 67-78.

Johler, J. R. (1966a), Zonal harmonics in low frequency terrestrial radio wave propagation, NBS Tech. Note 335.

Johler, J. R. (1966b), Theory of propagation of low frequency terrestrial radio waves--mathematical techniques for the interpretation of D-region propagation studies, Conference on Ground-Based Radio Wave Propagation Studies of the Lower Ionosphere, April 11-15, 1966, Radio Physics Laboratory, DRTE, Ottawa, Canada (to be published).

Johler, J. R. (1967), Propagation of an electromagnetic pulse from a nuclear burst, IEEE Trans. on Ant. and Prop., (to be published).

Johler, J. R., and L. A. Berry (1964), A complete mode sum for LF, VLF, ELF terrestrial radio wave fields, NBS Monograph 78.

Johler, J. R., and L. A. Berry (1965), On the effect of heavy ions on LF propagation, with special reference to a nuclear environment, NBS Tech. Note 313.

Johler, J. R. and J. D. Harper, Jr. (1962), Reflection and transmission of radio waves at a continuously stratified plasma with arbitrary magnetic induction, J. Res. NBS 66D (Radio Prop.), No. 1, 81-99.

Johler, J. R., and J. C. Morgenstern (1965), Propagation of the ground wave electromagnetic signal, with particular reference to a pulse of nuclear origin, Proc. IEEE 53, No. 12, 2043-2053.

U. S. Standard Atmosphere (1962), Superintendent of Documents, U. S. Govt. Printing Office, Washington, D. C. 20402.

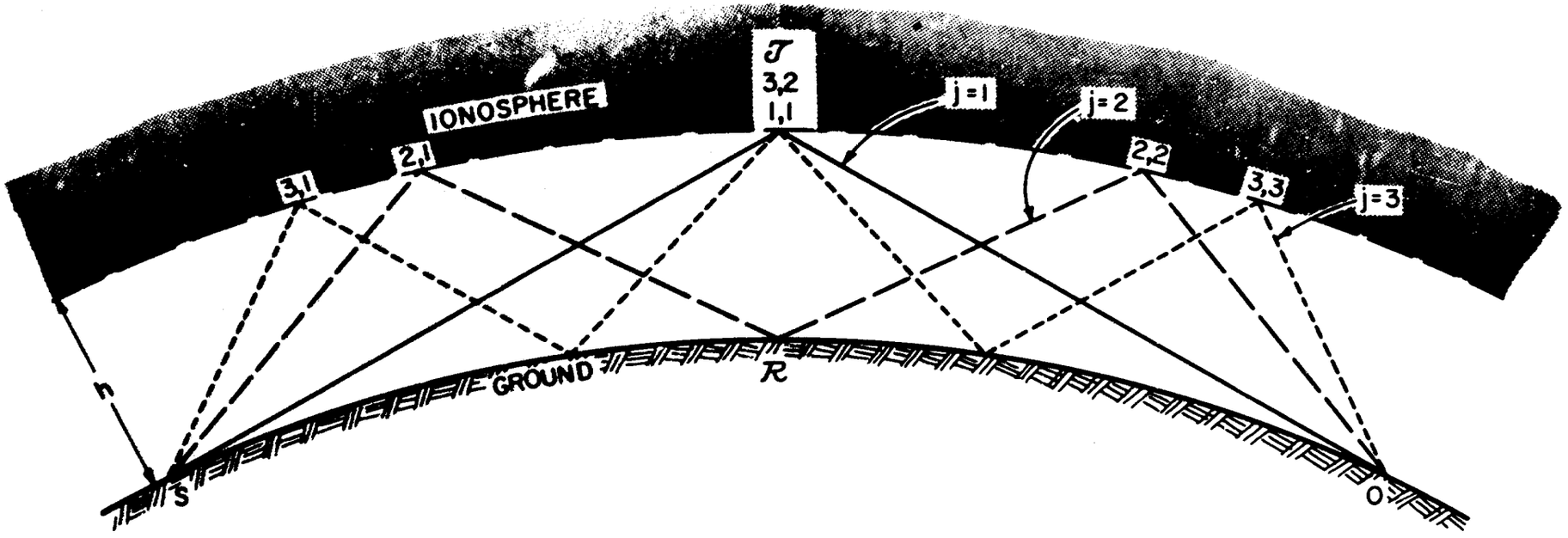

Figure 1. Illustrating approximate geometric-optical rays corresponding to terms of the rigorous geometric series for the theory of propagation in the terrestrial waveguide.

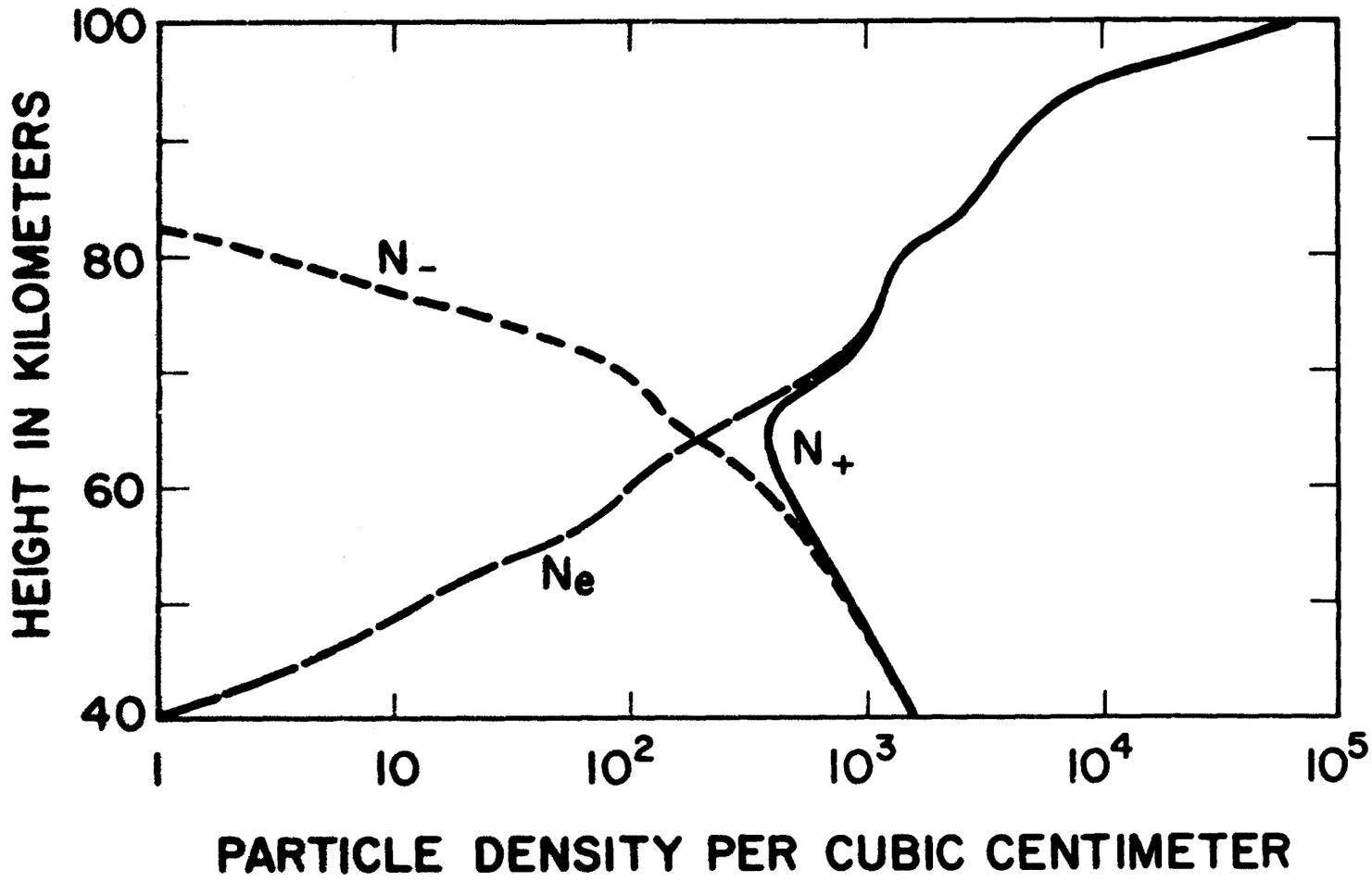

Figure 2. Illustrating typical daytime noon model of the ionosphere electrification (electrons or ions per cc) as a function of altitude. N_i refers to electrons, positive ions and negative ions for i = e, +, -, respectively.

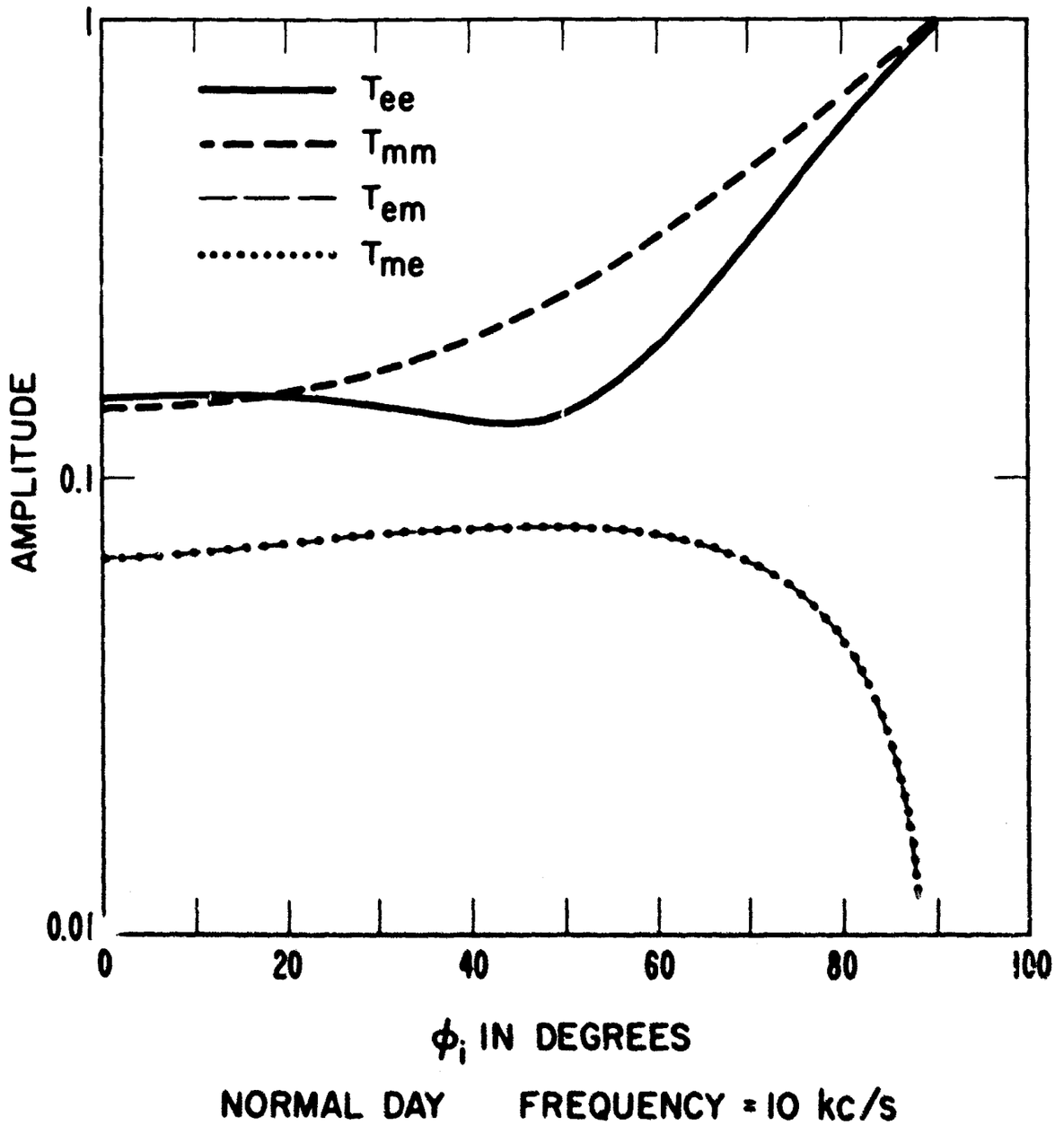

Figure 3. Amplitude of the ionosphere reflection coefficients as a function of the real part of the angle of incidence, φ_i, where $\cos \varphi_i$ is given by (2.9). $\varphi_a = 270°$, $I = 60°$, $N = 40$ A/m.

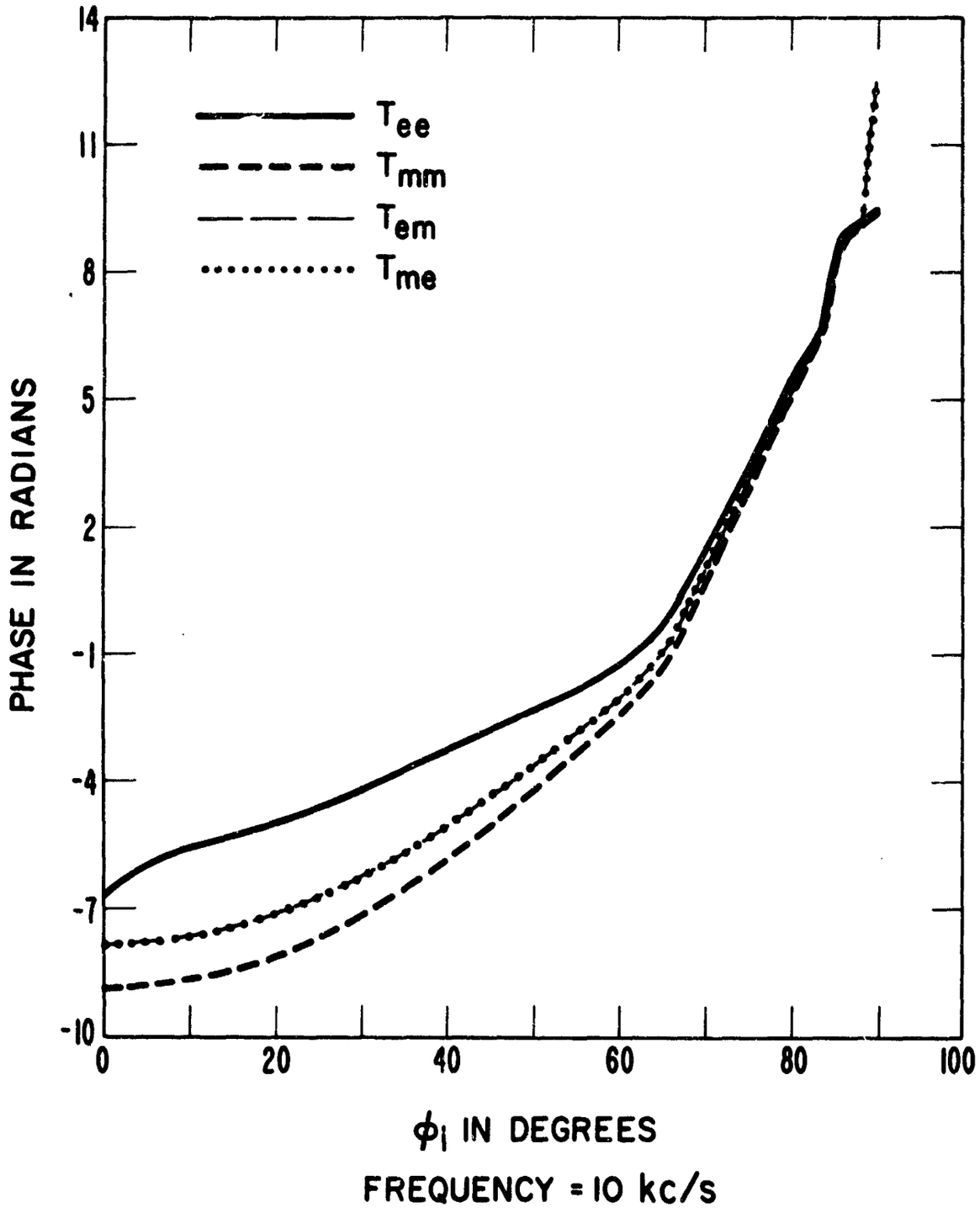

Figure 4. Phase of the ionosphere reflection coefficients as a function of the real part of the angle of incidence, φ_i, where cos φ_i is given by (2.9). φ_a = 270°, I = 60°, M = 40 A/m. The phase is referenced to a height, h = 40 km.

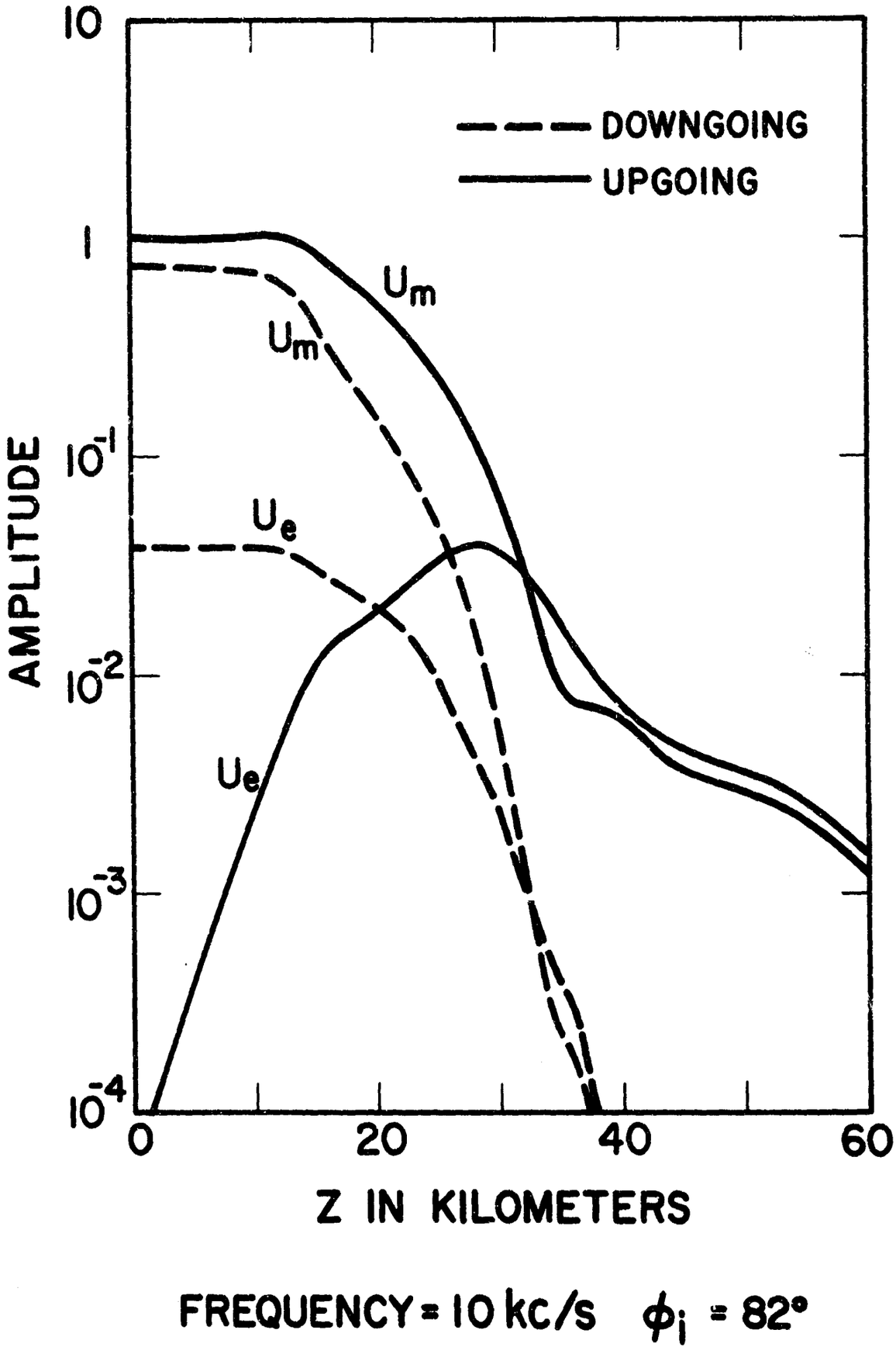

Figure 5. Transmission into the model ionosphere at 10 kc/s, depicting the amplitude of the transmission coefficients $|U_e|$, $|U_m|$.

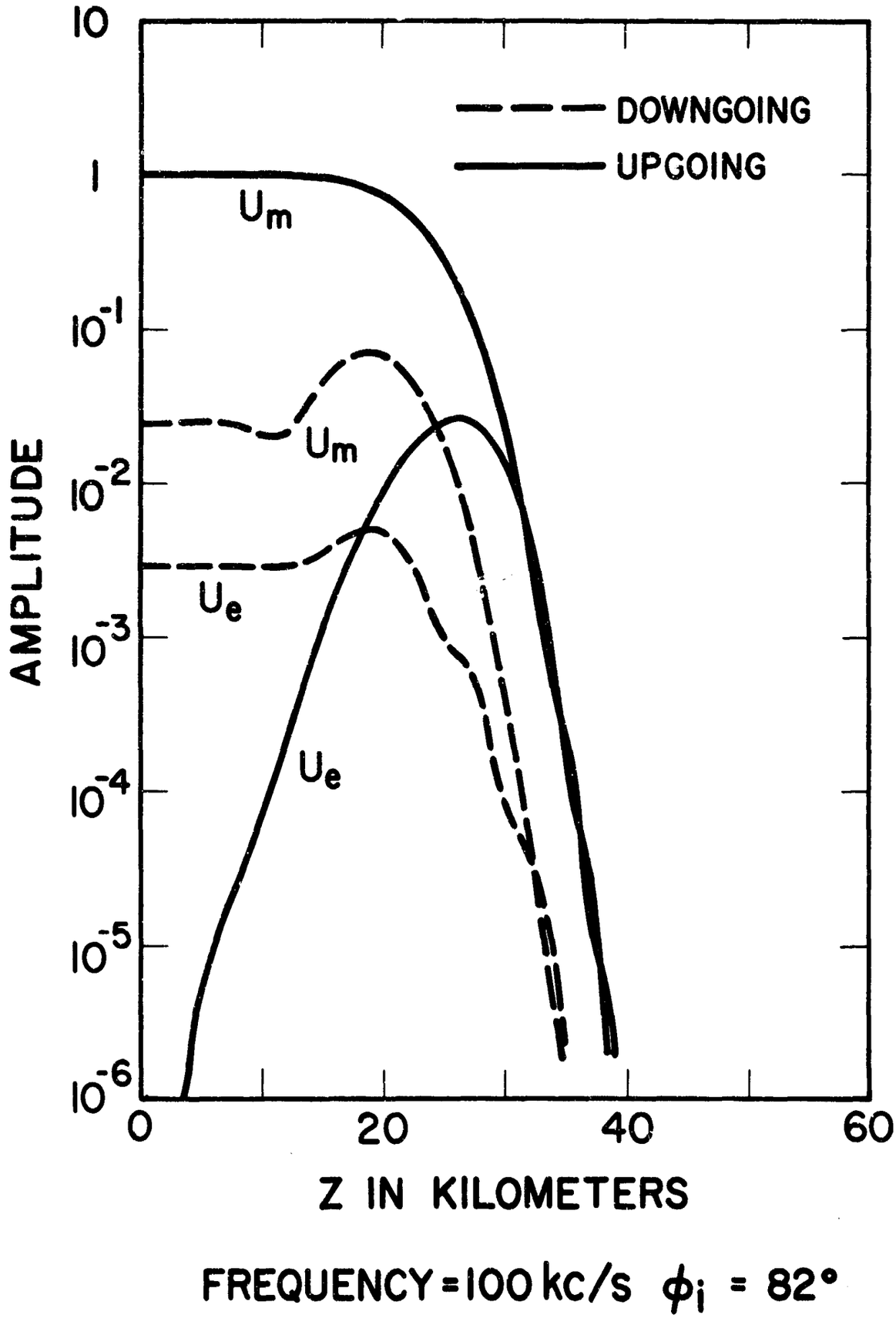

Figure 6. Transmission into the model ionosphere at 100 kc/s, depicting amplitude of the transmission coefficients $|U_e|$, $|U_m|$.

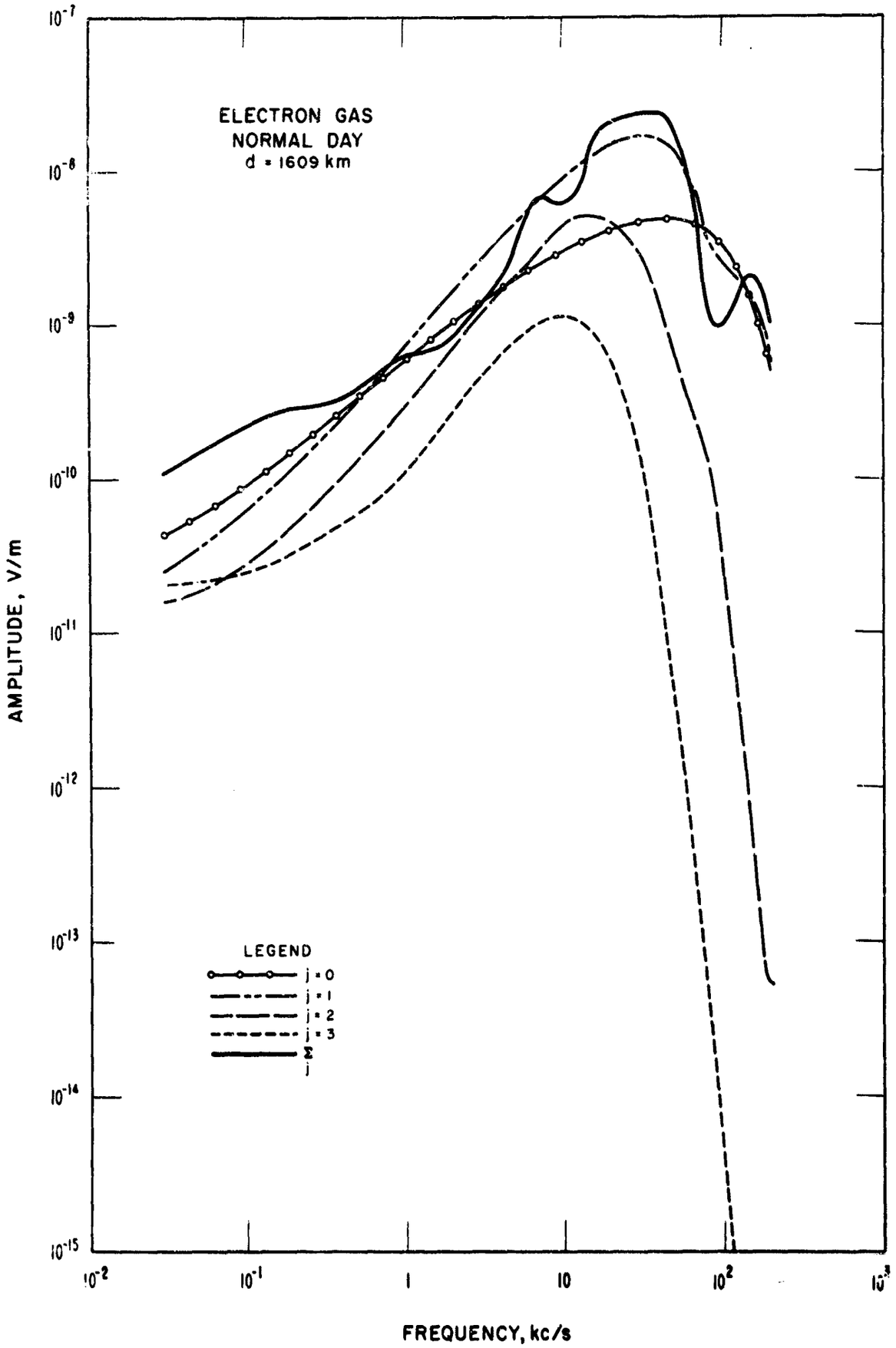

Figure 7. Amplitude of the normal propagation medium transform, $d = d_2 = 1609$ km; illustrating the terms of the geometric series $|E_j(\omega, d_2)|$ and the total field $\left|\sum_j E_j(\omega, d_2)\right|$.

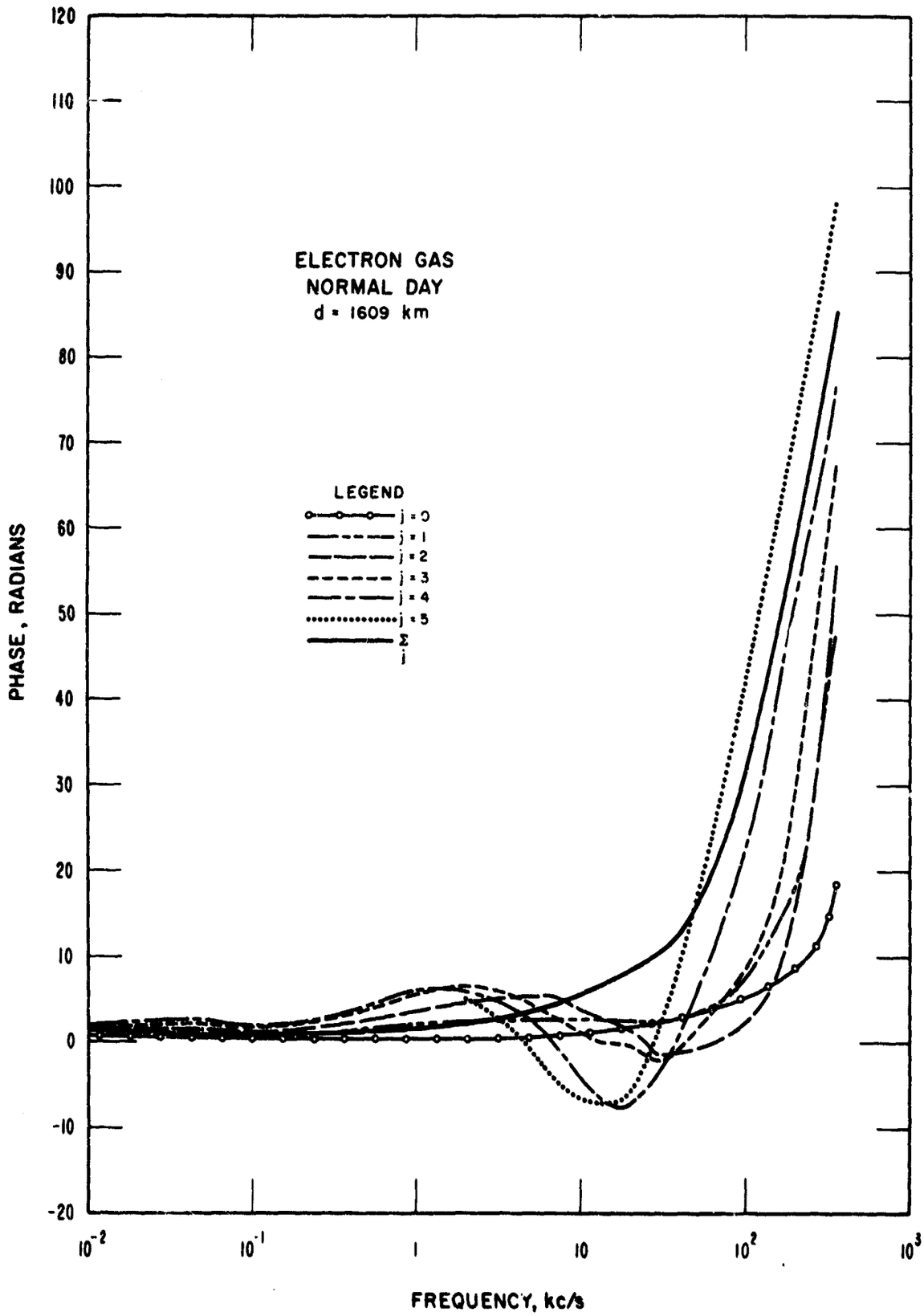

Figure 8. Phase of the normal propagation medium transform, $d = d_2 = 1609$ km; illustrating the terms of the geometric series $\text{Arg } E_j(\omega, d_2)$ and the total phase $\text{Arg} \sum_j E_j(\omega, d_2)$.

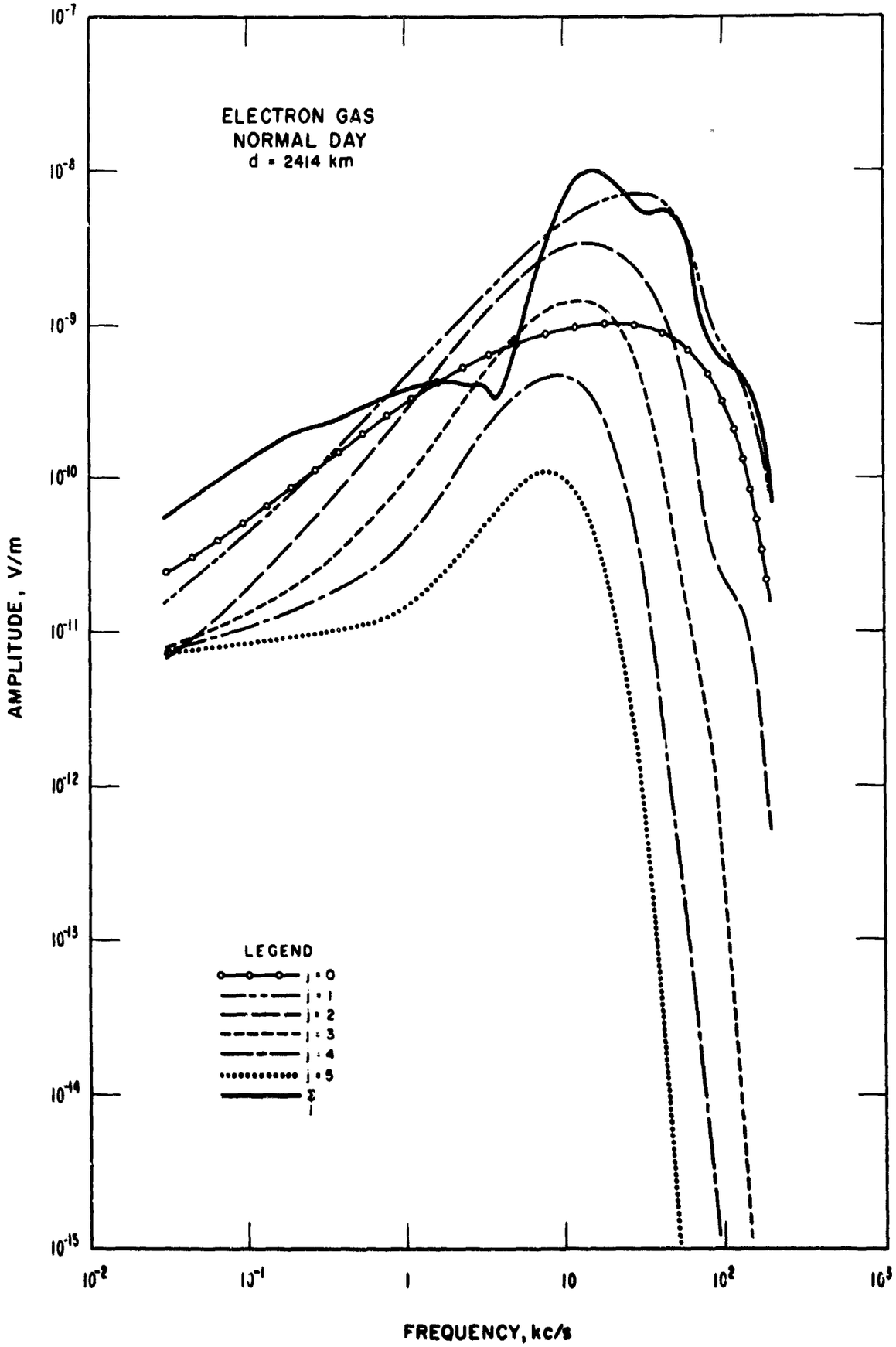

Figure 9. Amplitude of the normal propagation medium transform, $d = d_2 = 2414$ km; illustrating the terms of the geometric series $|E_j(\omega, d_2)|$ and the total field $\left|\sum_j E_j(\omega, d_2)\right|$.

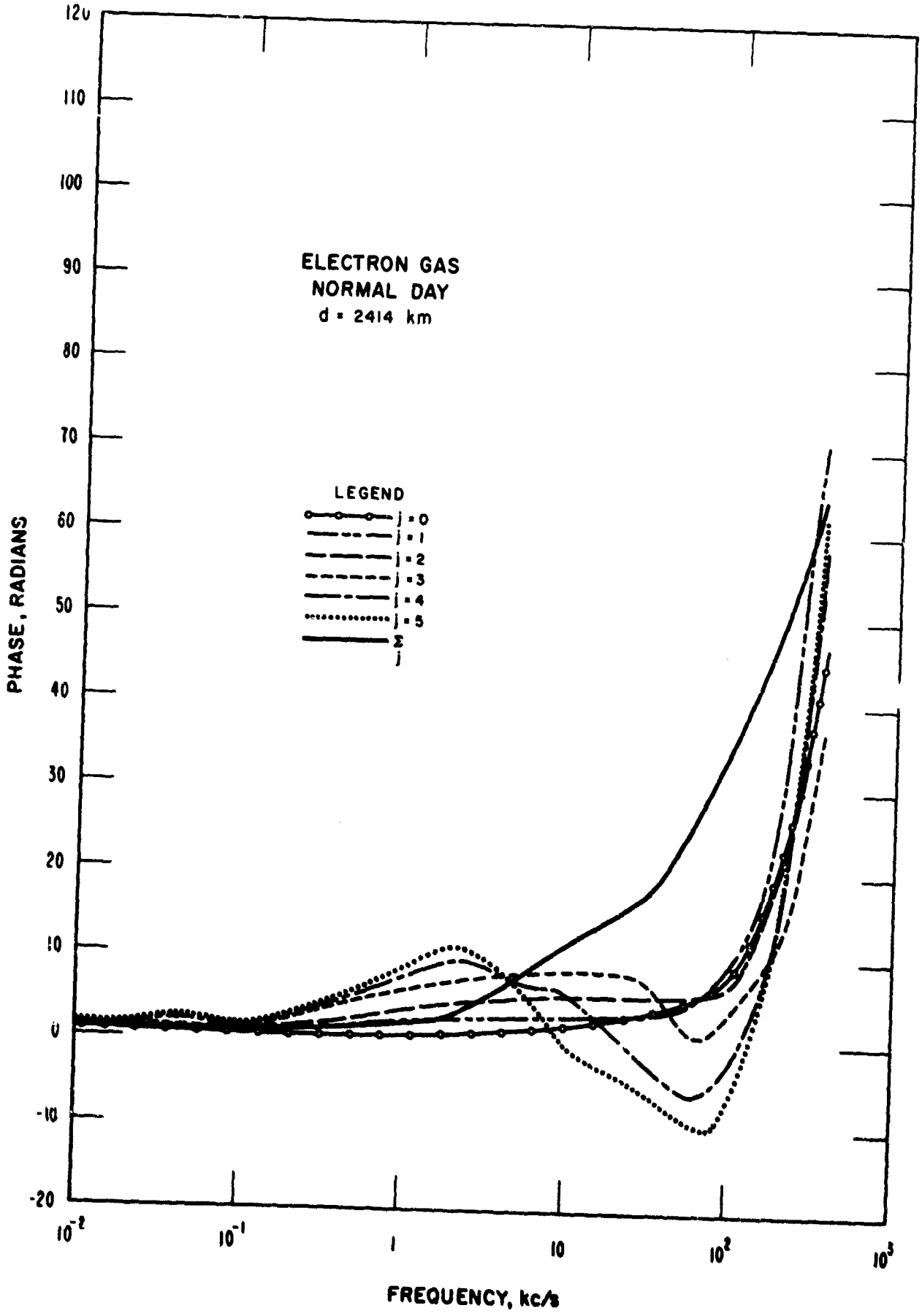

Figure 10. Phase of the normal propagation medium transform, $d = d_2 = 2414$ km; illustrating the terms of the geometric series Arg $E_j(\omega, d_2)$ and the total phase Arg $\sum_j E_j(\omega, d_2)$.

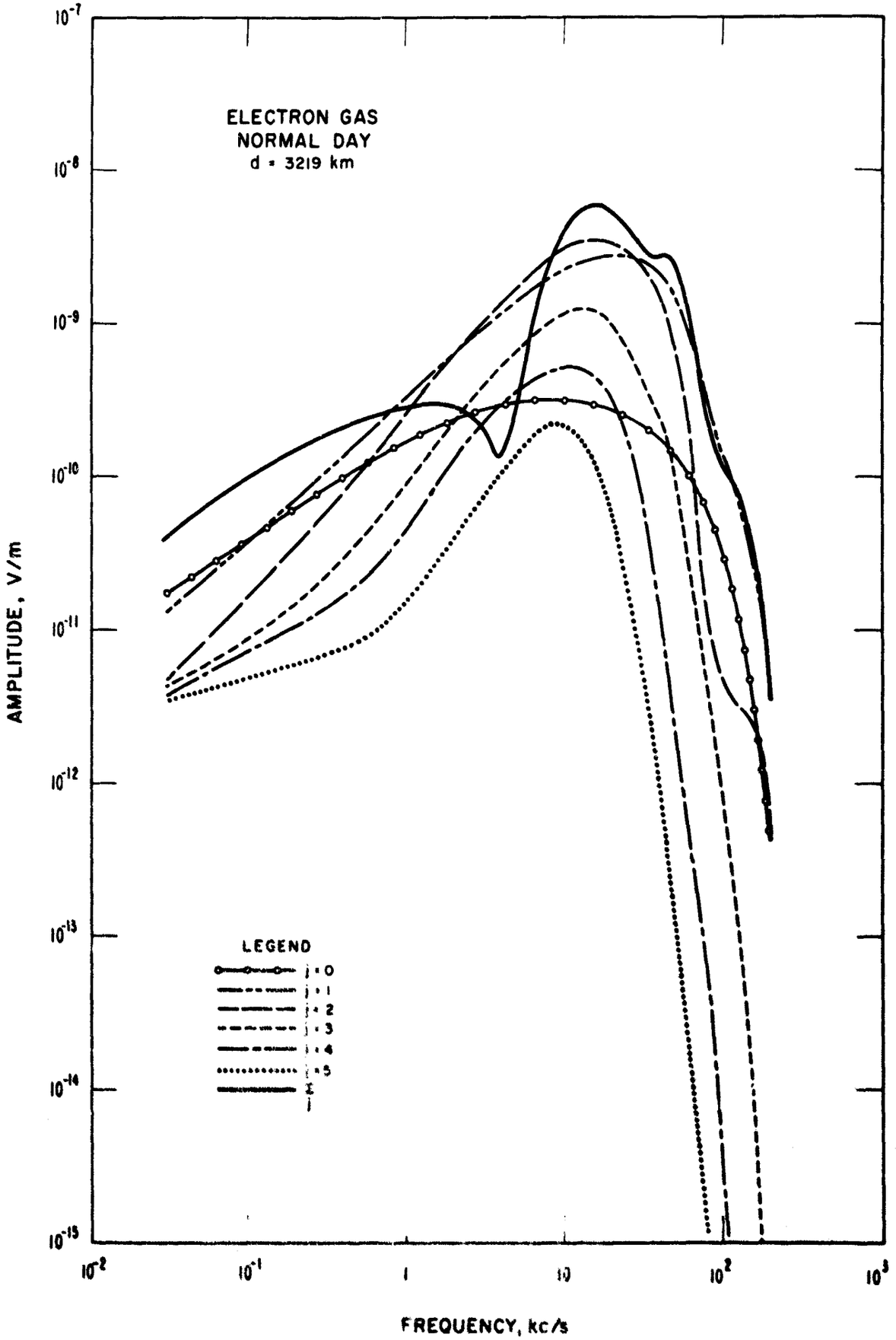

Figure 11. Amplitude of the normal propagation medium transform, $d = d_2 = 3219$ km; illustrating the terms of the geometric series $|E_j(\omega, d_2)|$ and the total field $\left|\sum_j E_j(\omega, d_2)\right|$.

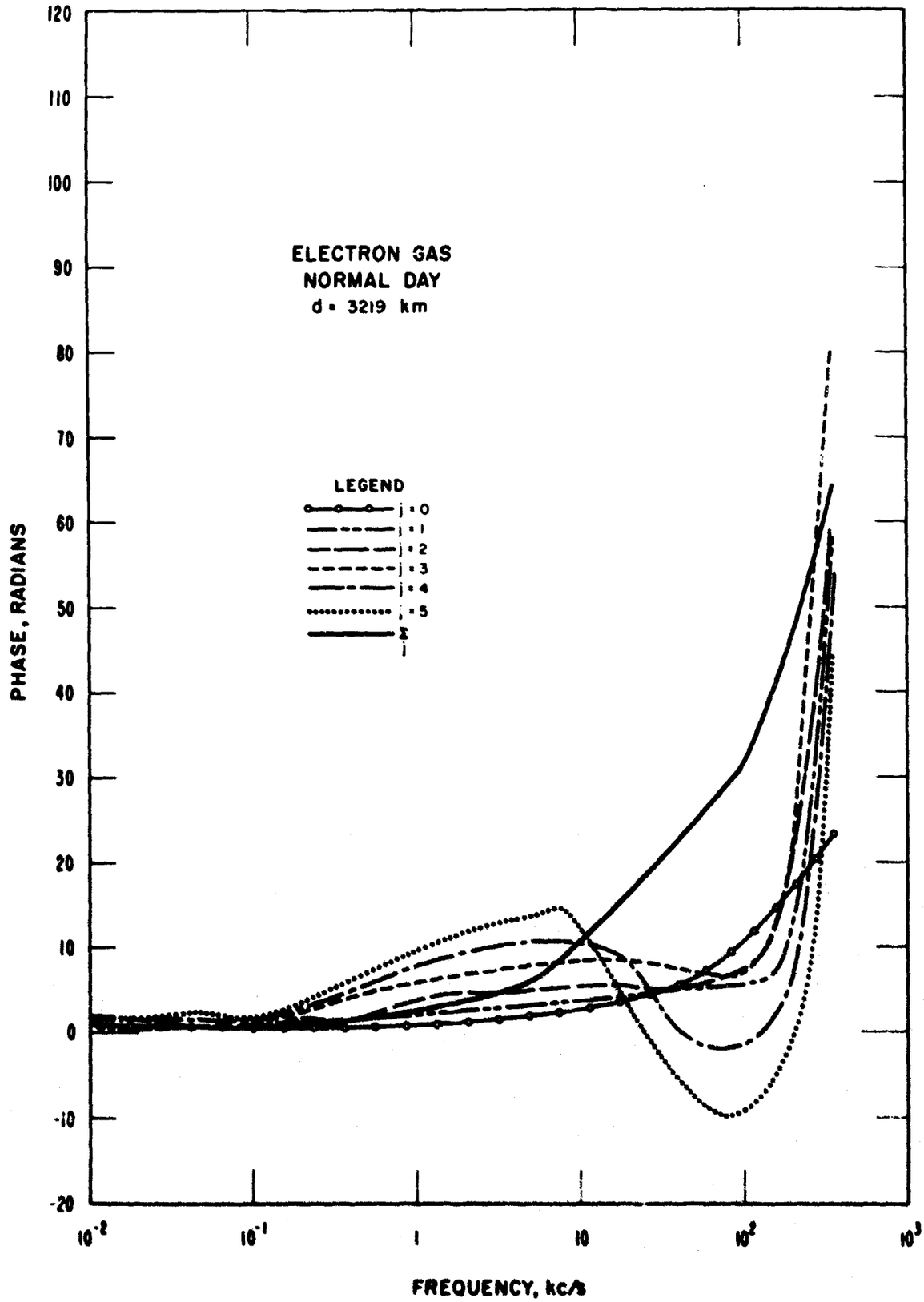

Figure 12. Phase of the normal propagation medium transform, $d = d_g = 3219$ km, illustrating the terms of the geometric series Arg $E_j(\omega, d_g)$ and the total phase Arg $\sum_j E_j(\omega, d_g)$.

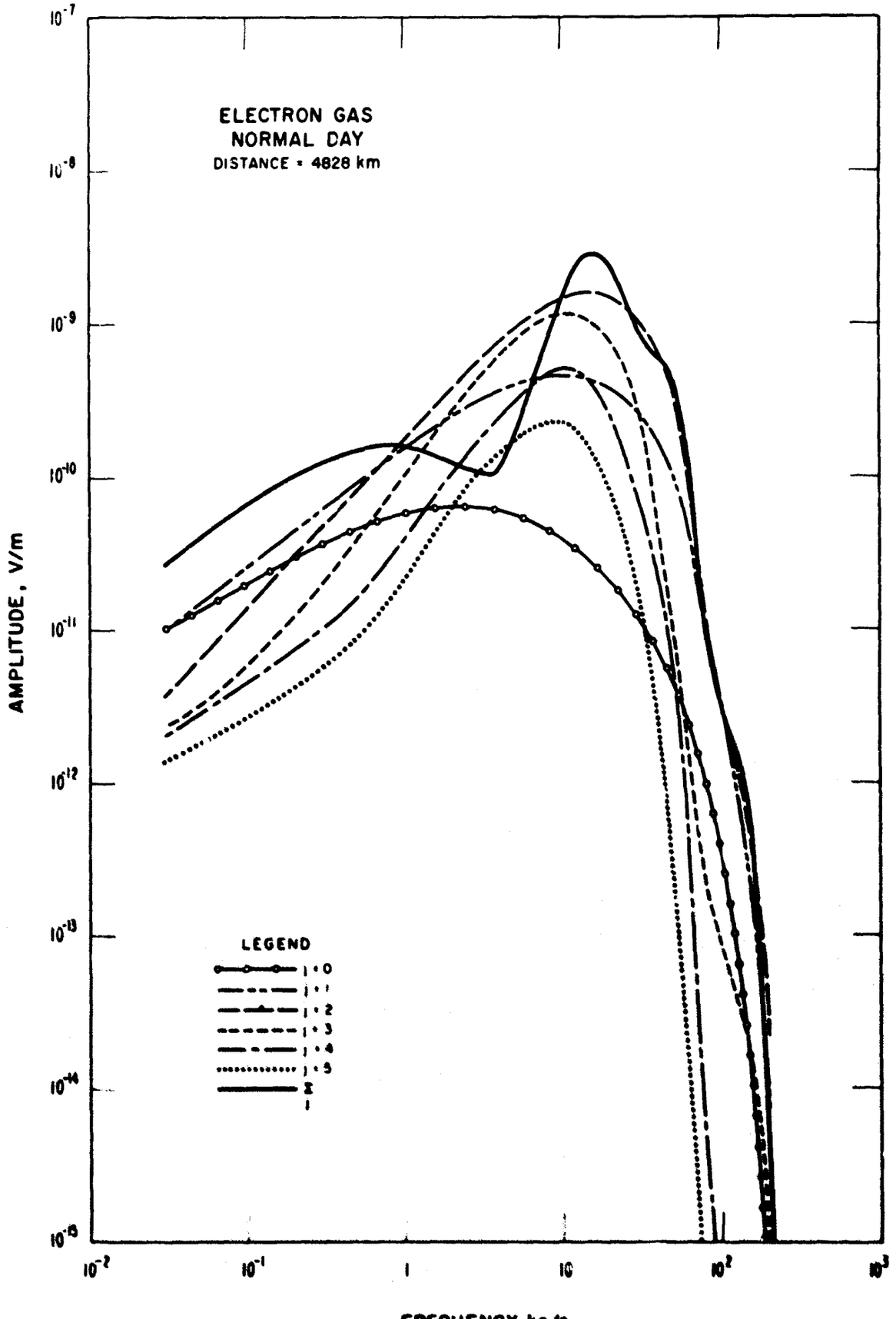

Figure 13. Amplitude of the normal propagation medium transform, $d = d_2 = 4828$ km; illustrating the terms of the geometric series $|E_j(\omega, d_2)|$ and the total field $\left|\sum_j E_j(\omega, d_2)\right|$.

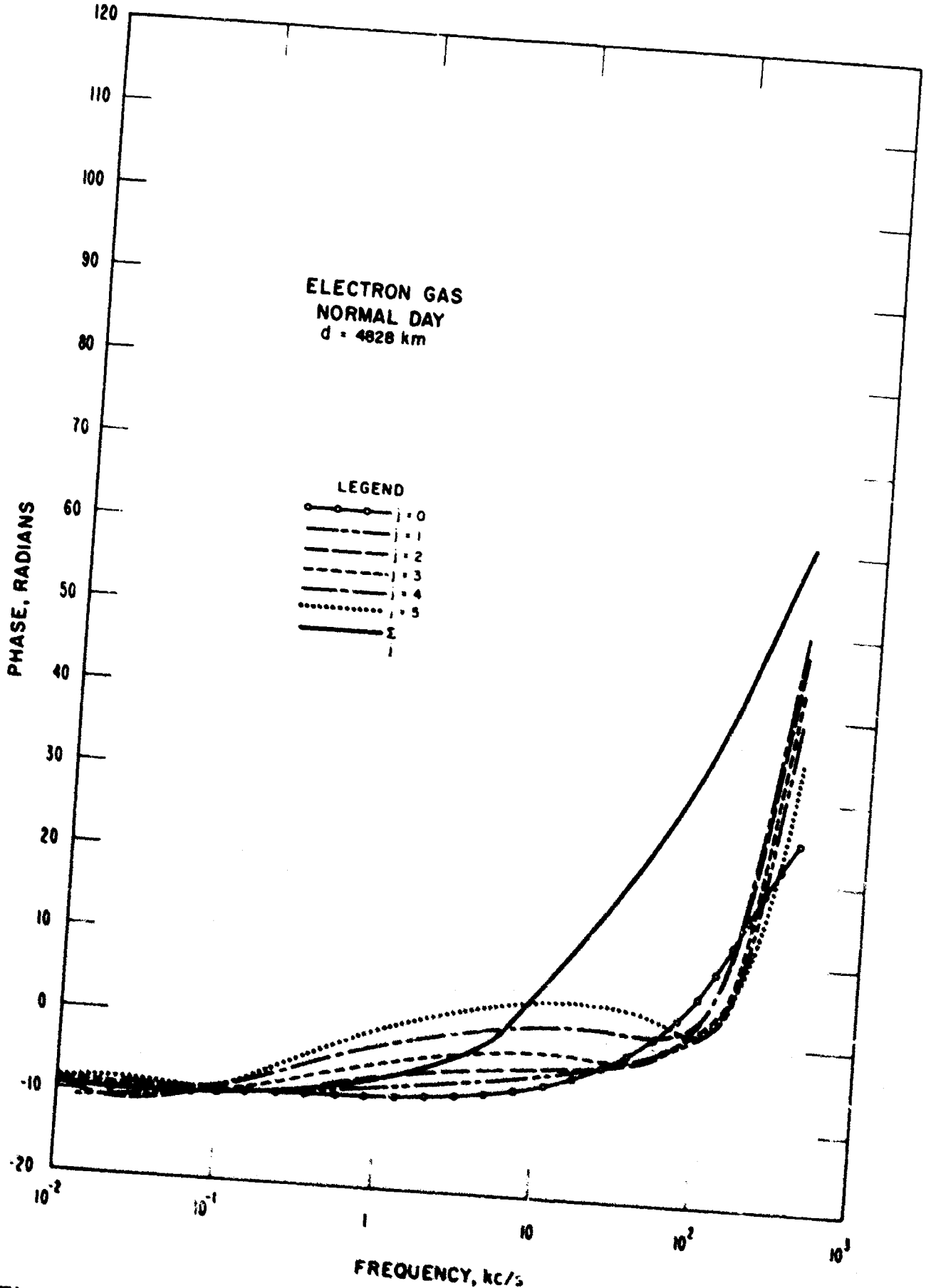

Figure 14. Phase of the normal propagation medium transform, $d = d_2 = 4828$ km; illustrating the terms of the geometric series Arg $E_j(w, d_2)$ and the total phase Arg $\sum_j E_j(w, d_2)$.

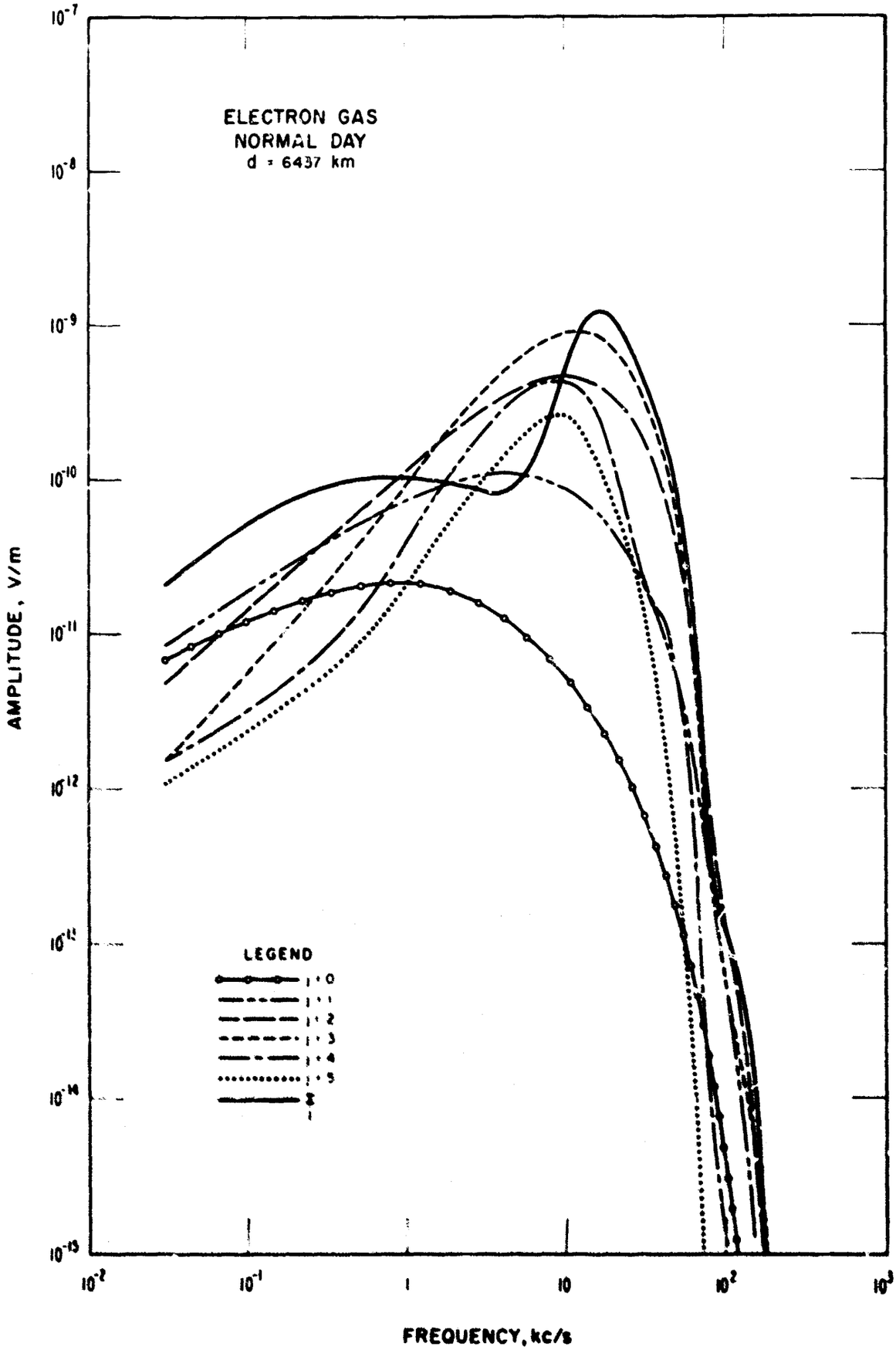

Figure 15. Amplitude of the normal propagation medium transform, $d = d_2 = 6437$ km, illustrating the terms of the geometric series $|E_j(\omega, d_2)|$ and the total field $\left|\sum_j E_j(\omega, d_2)\right|$.

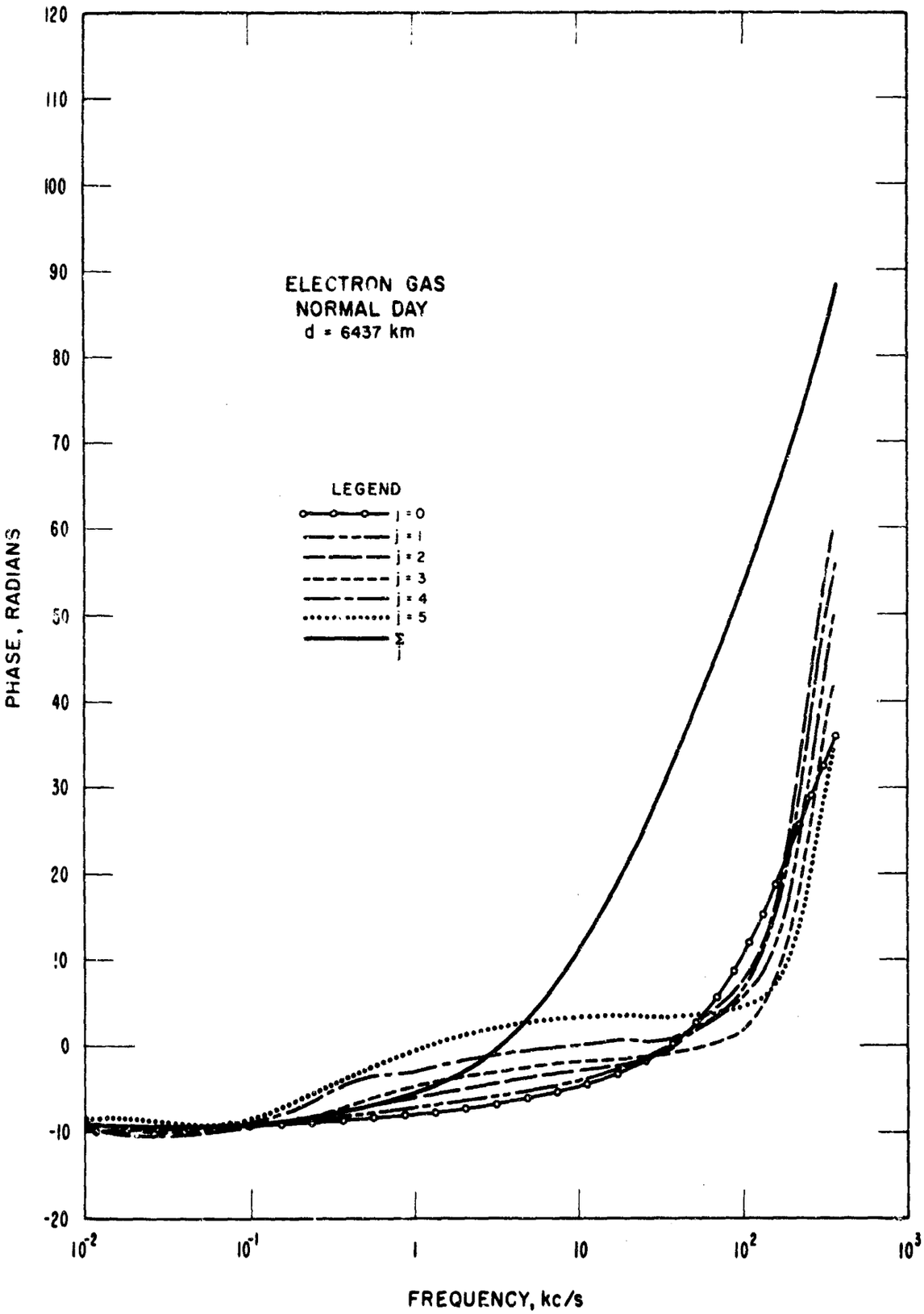

Figure 16. Phase of the normal propagation medium transform, $d = d_2 = 6437$ km; illustrating the terms of the geometric series Arg $E_j(\omega, d_2)$ and the total phase Arg $\sum_j E_j(\omega, d_2)$.

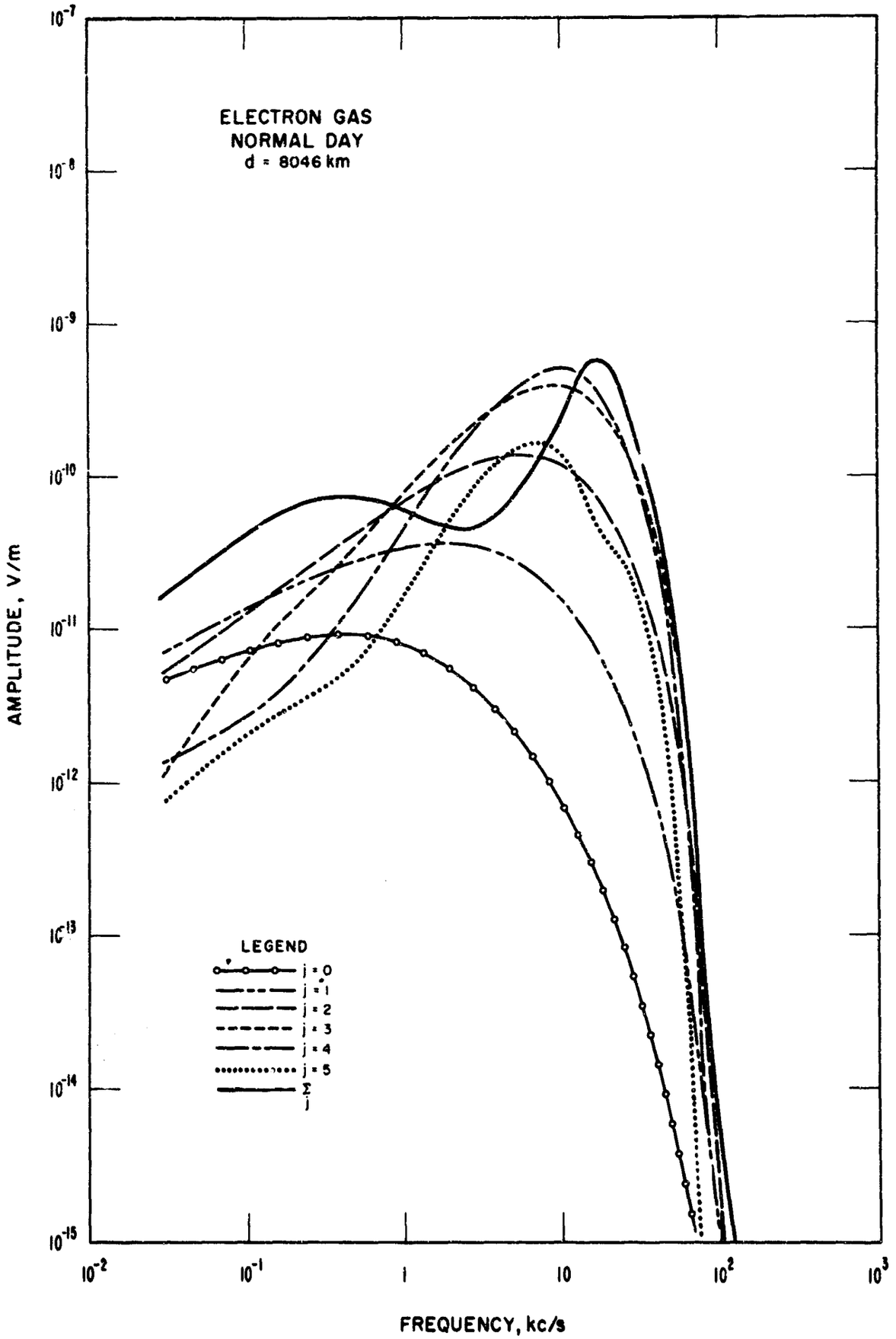

Figure 17. Amplitude of the normal propagation medium transform, $d = d_\oplus = 8046$ km; illustrating the terms of the geometric series $|E_j(\omega, d_\oplus)|$ and the total field $\left|\sum_j E_j(\omega, d_\oplus)\right|$.

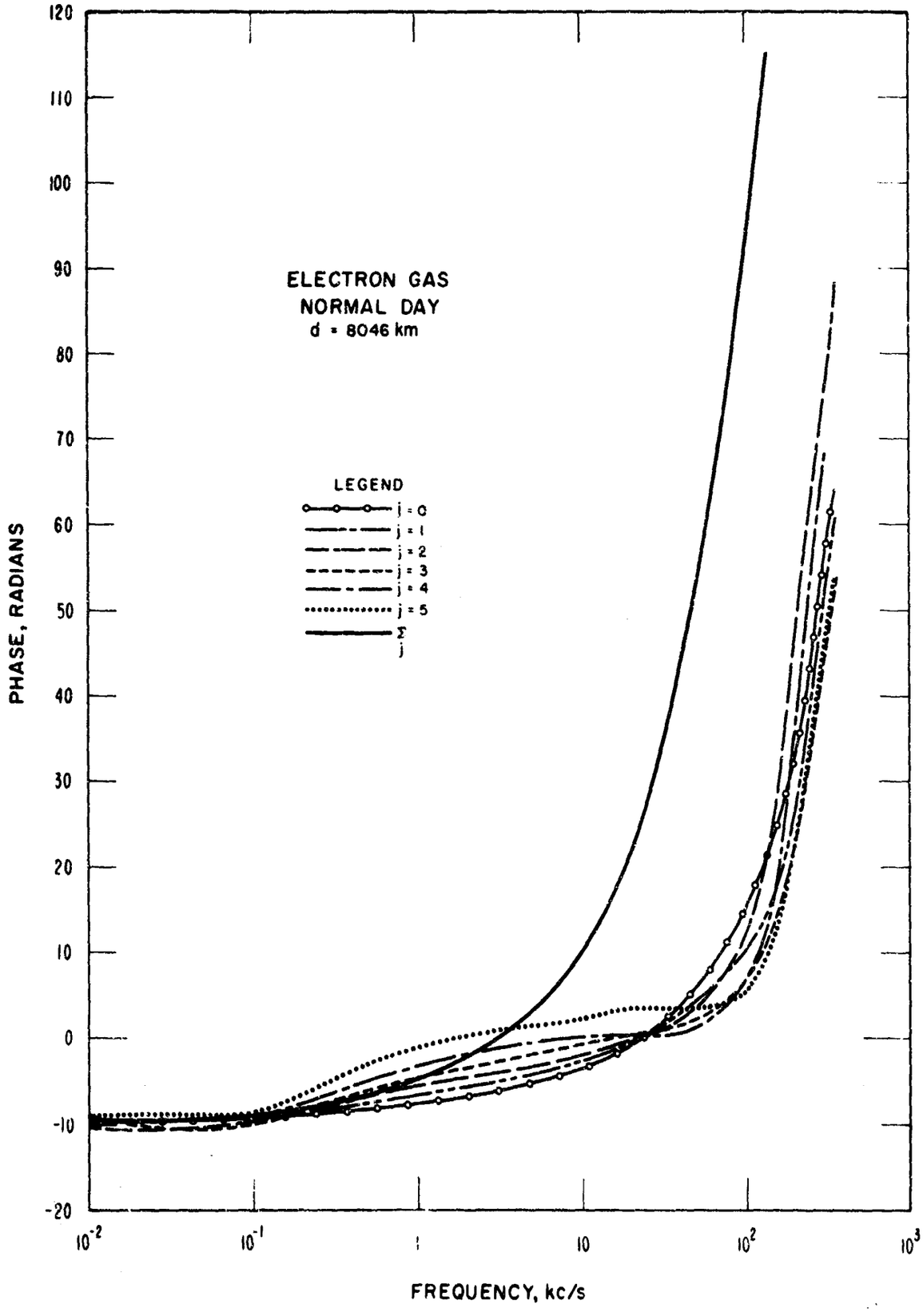

Figure 18. Phase of the normal propagation medium transform, $d = d_2 = 8046$ km; illustrating the terms of the geometric series Arg $E_j(\omega, d_2)$ and the total phase Arg $\sum_j E_j(\omega, d_2)$.

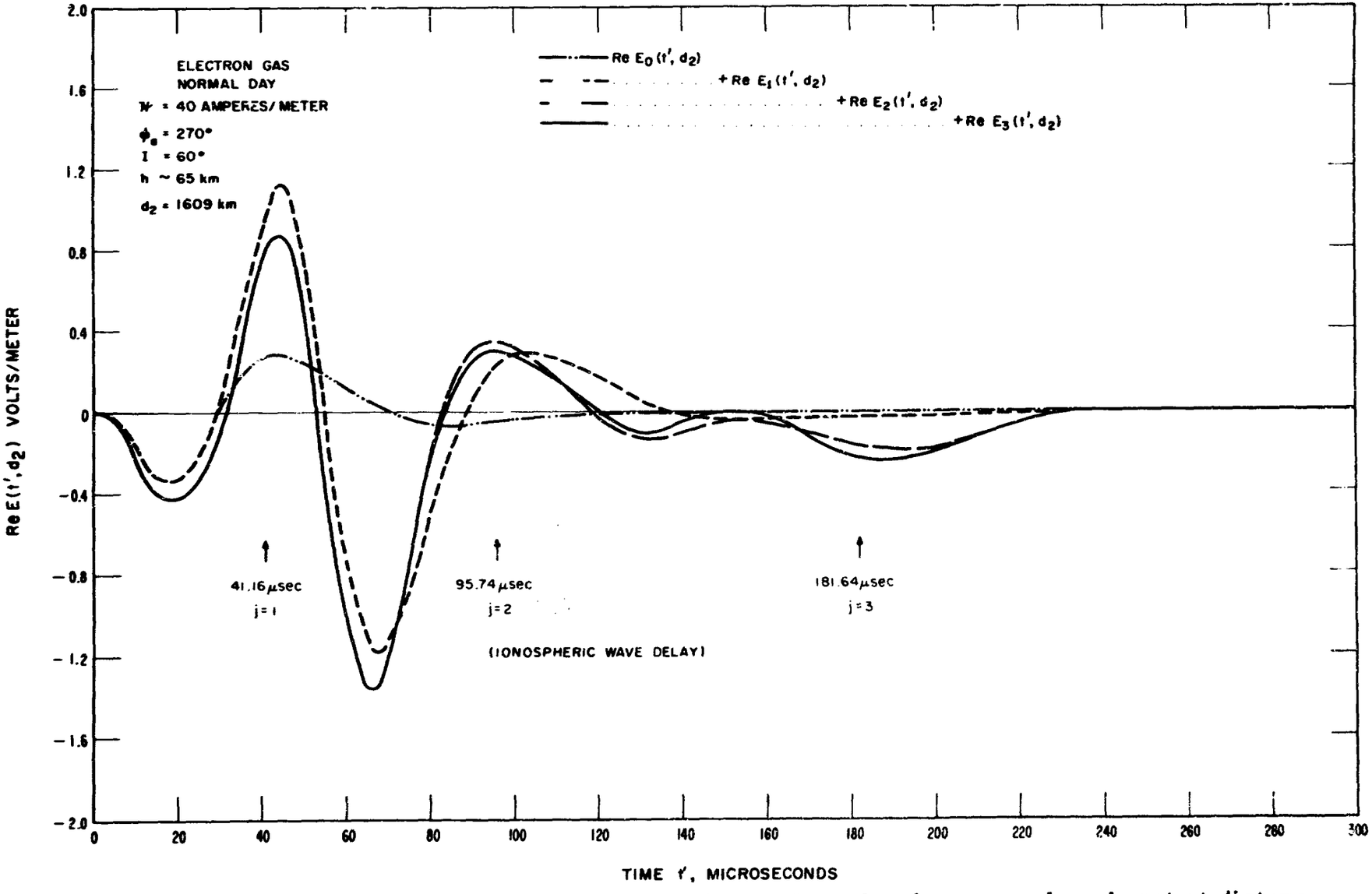

Figure 19. Illustrating theoretical reconstruction of the pulse from a nuclear burst at distance, d = 1609 km, as a sum of pulses in the time domain, where each component pulse corresponds to a term of the geometric series, j = 0, 1, 2, 3 · · ·.

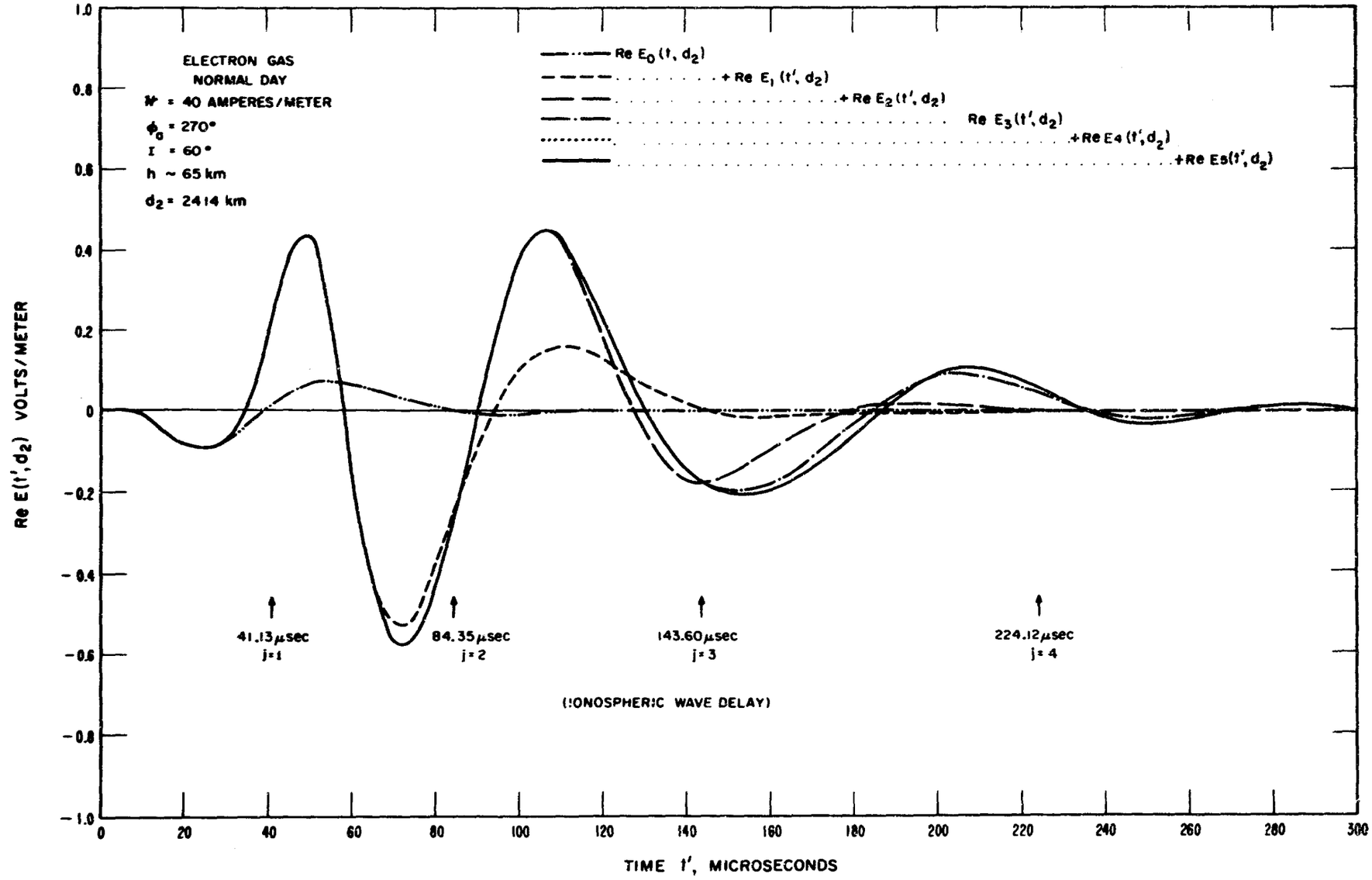

Figure 20. Illustrating theoretical reconstruction of the pulse from a nuclear burst at distance, d = 2414 km, as a sum of pulses in the time domain where each component pulse corresponds to a term of the geometric series, j = 0, 1, 2, 3···.

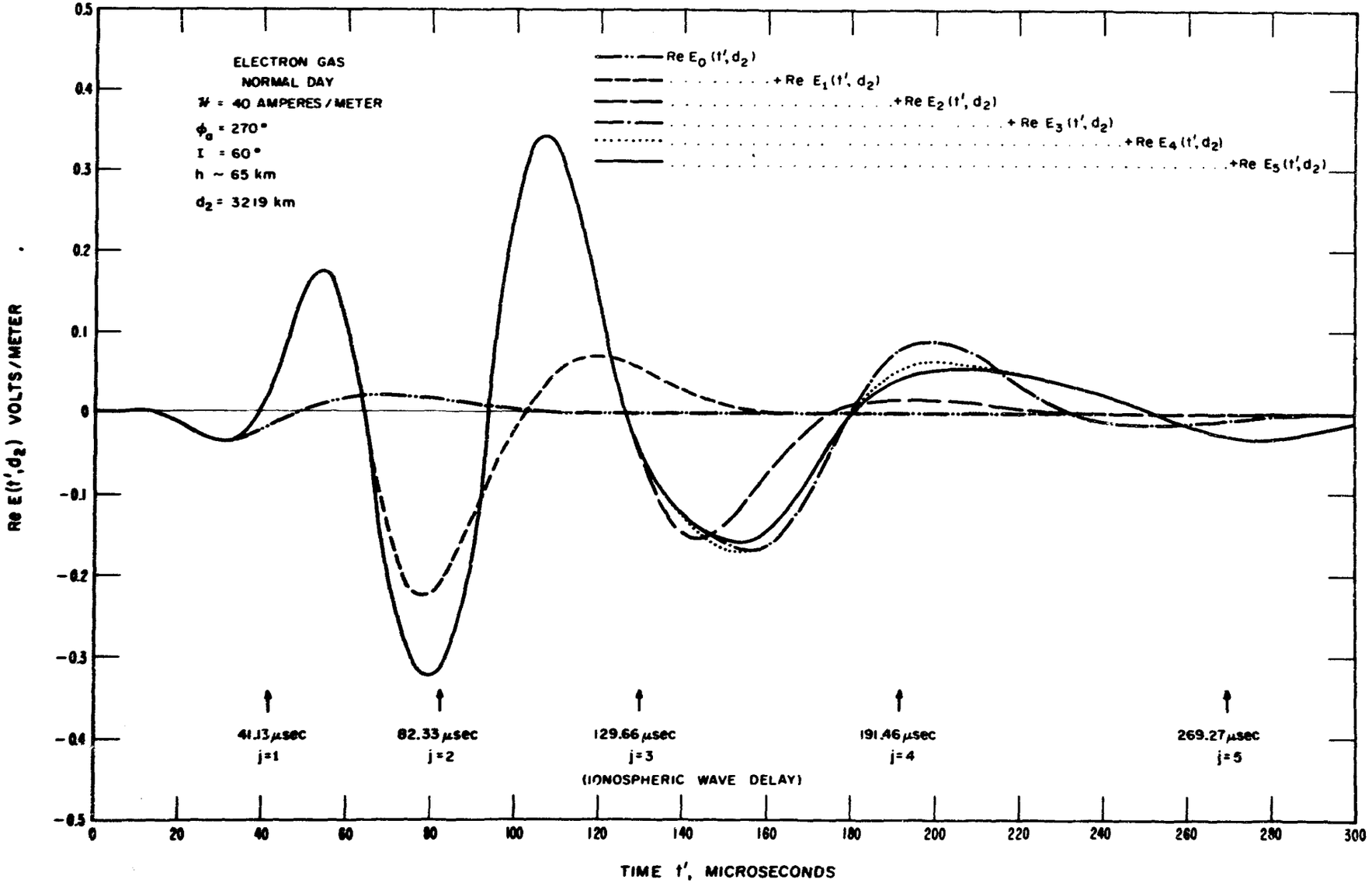

Figure 21. Illustrating theoretical reconstruction of the pulse from a nuclear burst at distance, d = 3219 km, as a sum of pulses in the time domain, where each component pulse corresponds to a term of the geometric series, j = 0, 1, 2, 3 · · ·.

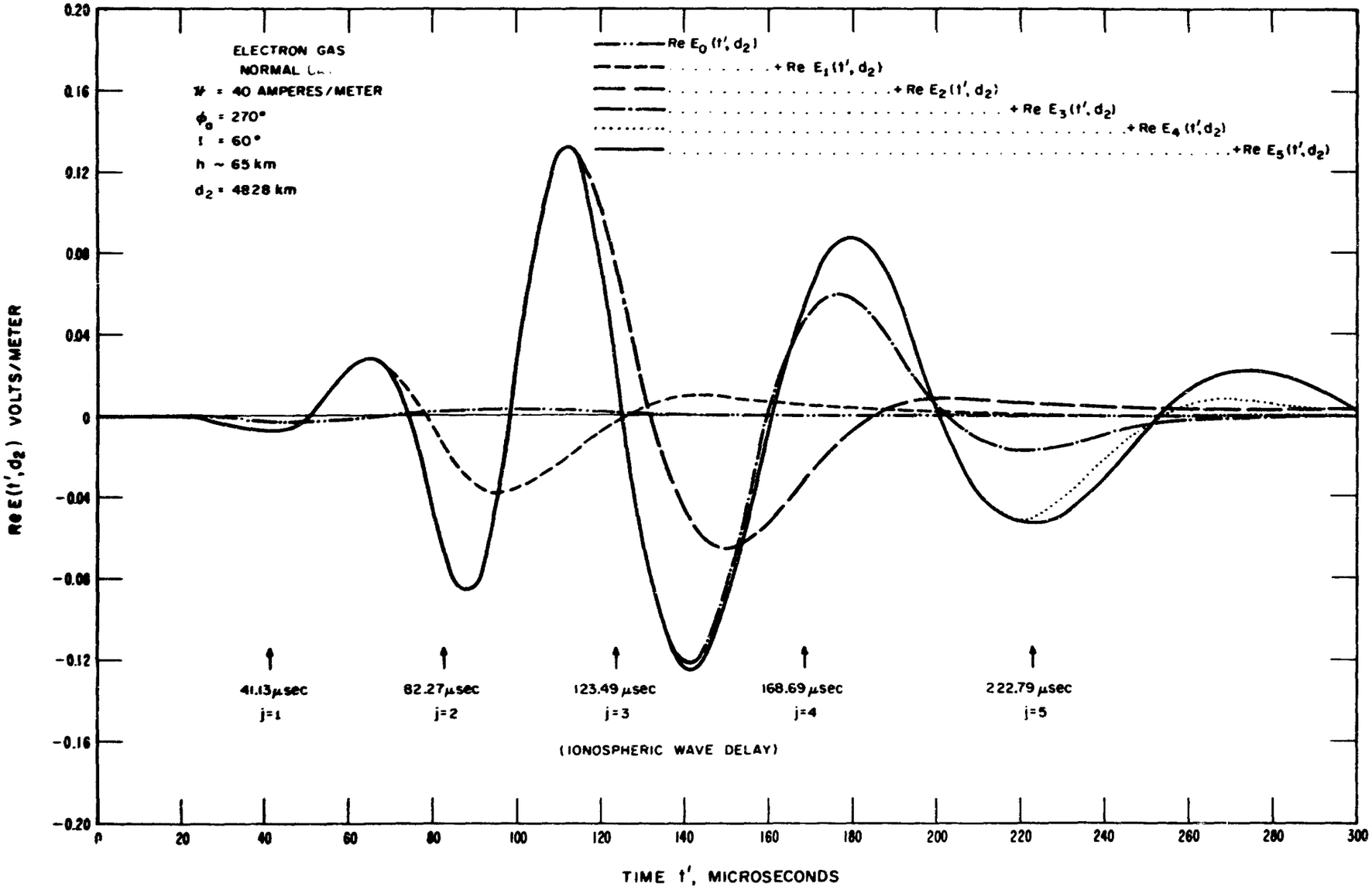

Figure 22. Illustrating theoretical reconstruction of the pulse from a nuclear burst at distance, d = 4828 km, as a sum of pulses in the time domain where each component pulse corresponds to a term of the geometric series, j = 0, 1, 2, 3 · · ·.

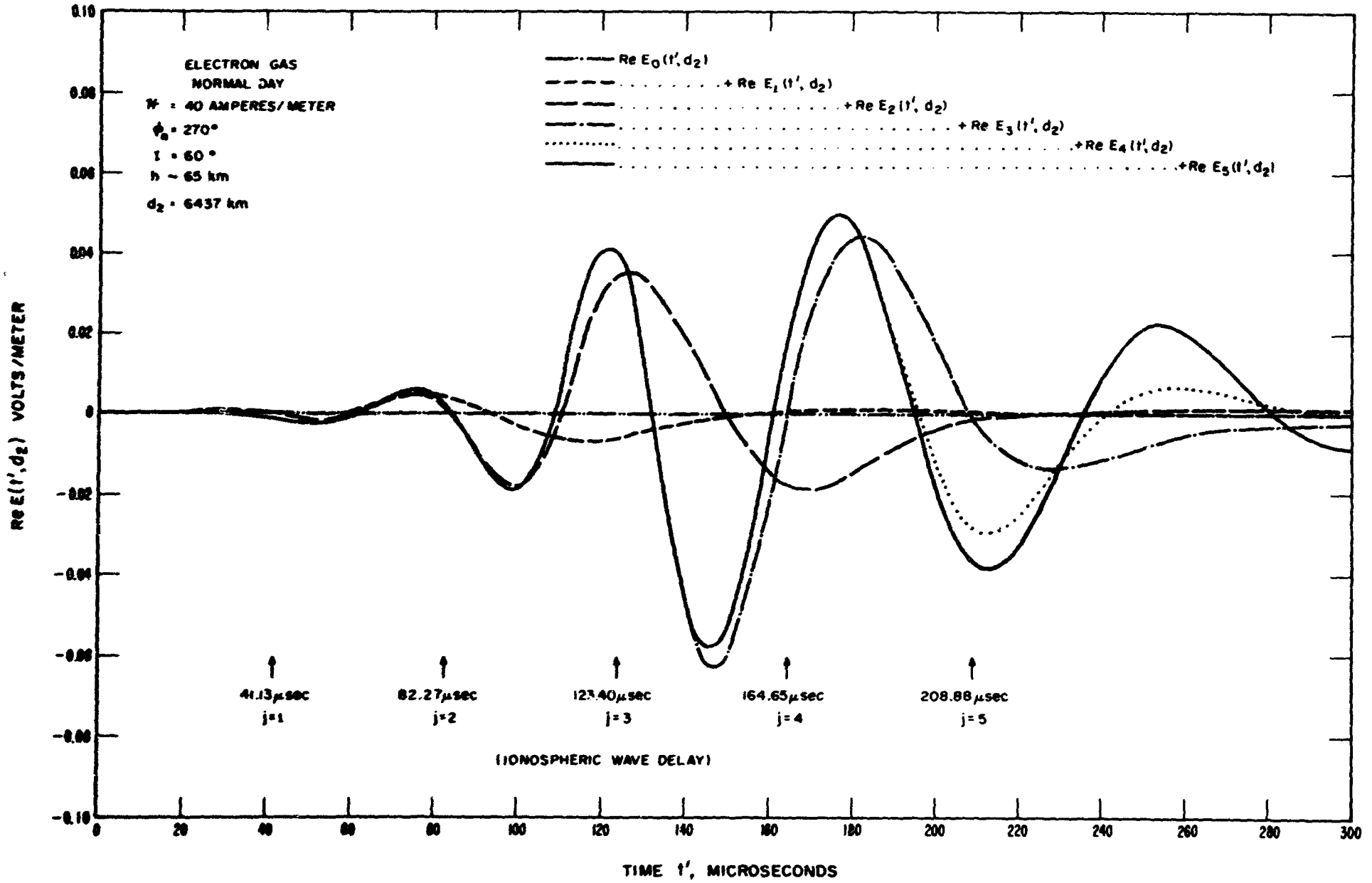

Figure 23 Illustrating theoretical reconstruction of the pulse from a nuclear burst at distance, d = 6437 km, as a sum of pulses in the time domain where each component pulse corresponds to a term of the geometric series, j = 0, 1, 2, 3 · · ·.

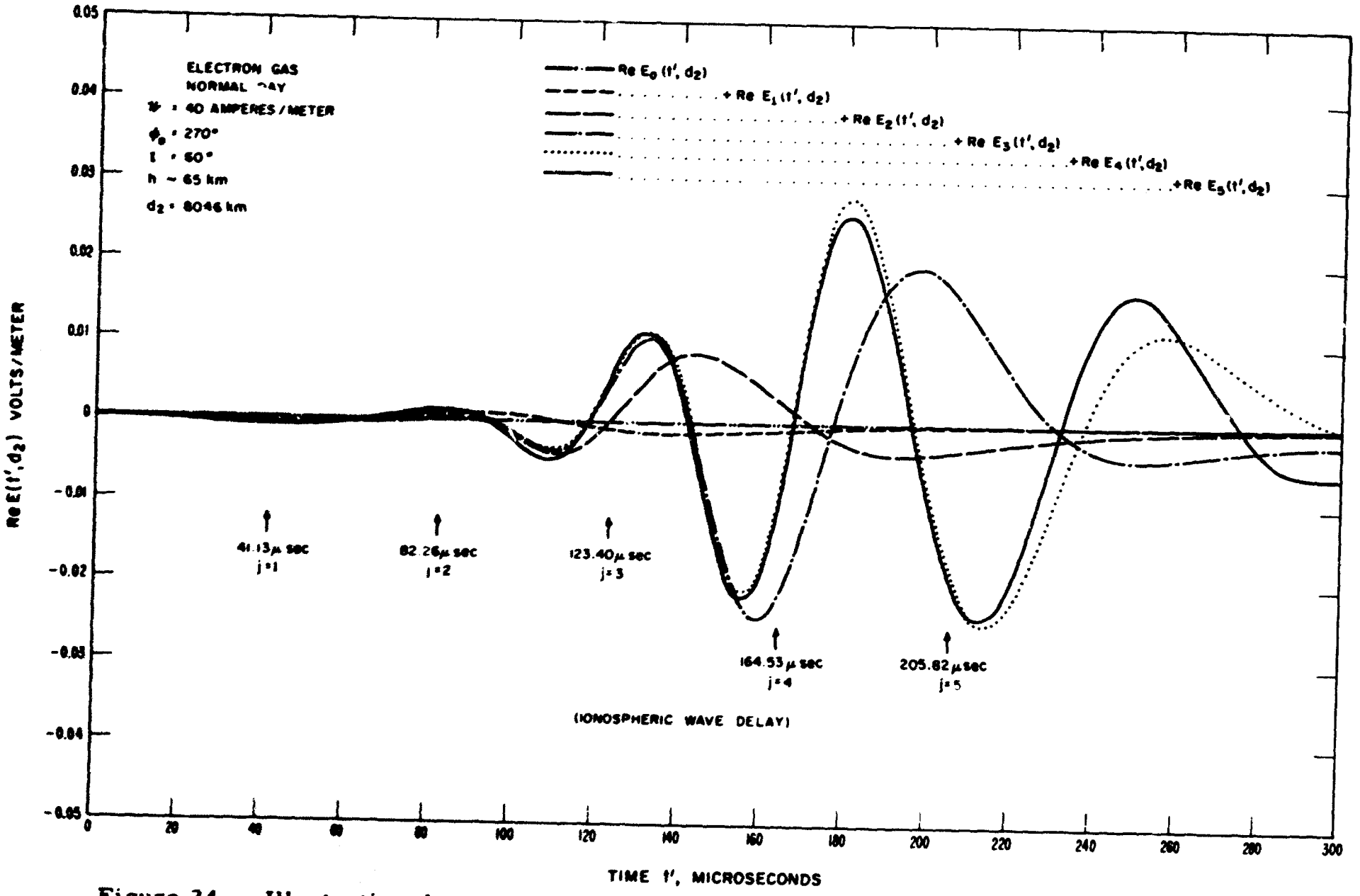

Figure 24. Illustrating theoretical reconstruction of the pulse from a nuclear burst at distance, d = 8046 km, as a sum of pulses in the time domain, where each component pulse corresponds to a term of the geometric series, j = 0, 1, 2, 3 · · · .

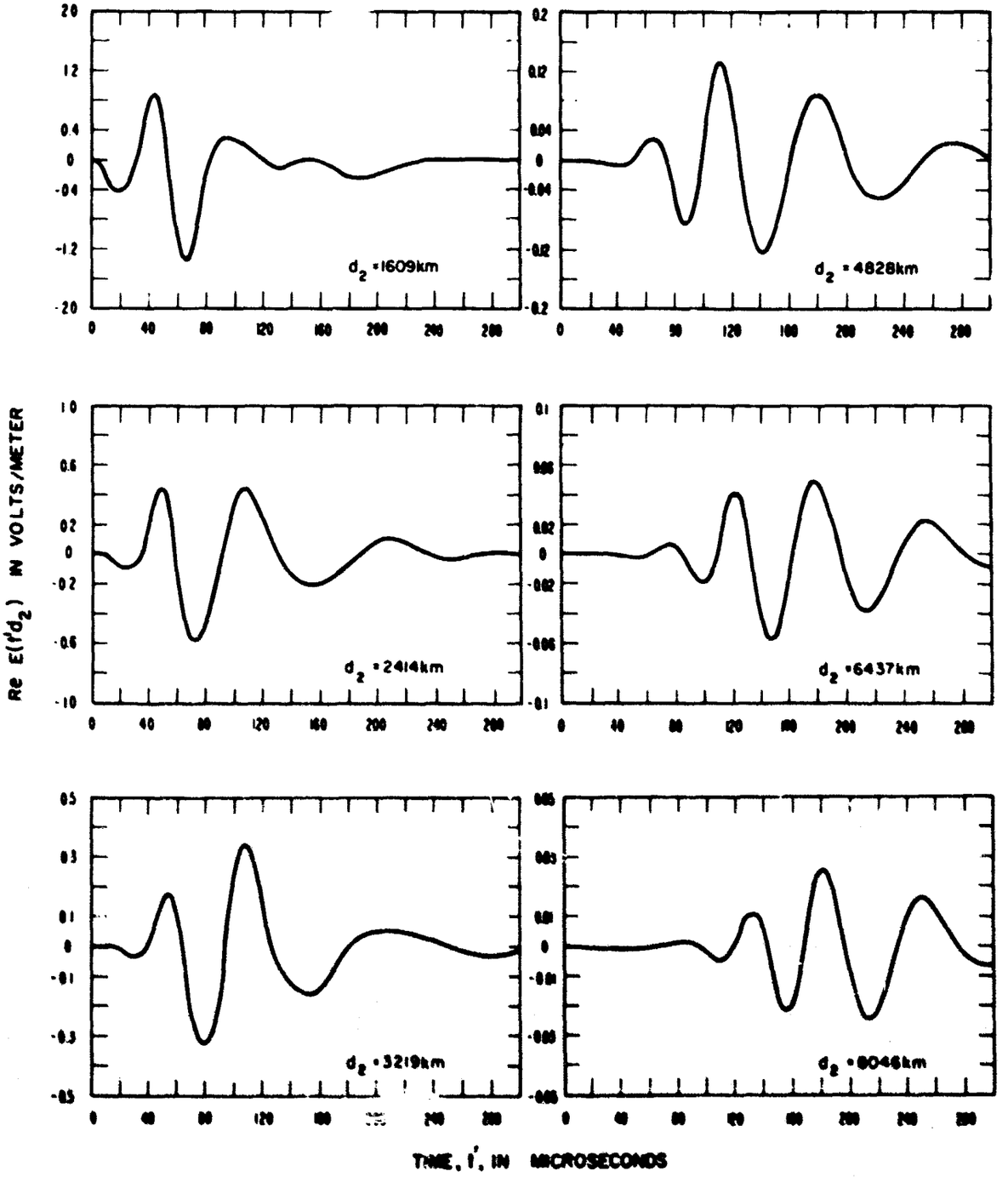

Figure 25. Pulse propagated theoretically from a nuclear burst to various distances between 1609 and 8046 km, illustrating the change in form or shape of the pulse as a consequence of the filtering action of the propagation medium.